Northeastern University

Boston, Massachusetts

Annual Report on

The Study of Optical Properties and Collective

Oscillations in New Solid State Materials as a

Function of Temperature Using Infrared and Raman Techniques

Period. 15 May 1969-14 May 1970

NASA Grant #NGL 22-011-051

Submitted by

Clive H. Perry

Clive H. Perry

CASE FILE
COPY

Prepared for   National Aeronautics and Space Administration
               Office of Scientific and Technical Information (Code US)
               Washington, D.C. 20546

This report is intended for the internal management use of the Grantee and
the National Aeronautics and Space Administration.

ABSTRACT

A temperature dependent study of the vibrations of crystal lattices and low-lying electronic states has been undertaken using infrared and Raman light scattering techniques. The emphasis has been placed on new materials which have useful applications such as low temperature filters for long-wave infrared radiation, new laser host-crystals, crystals as electro-optic devices and nonlinear effects. The materials of interest have included various ferroelectrics (and antiferroelectrics), piezoelectrics, antiferromagnets, certain semiconductors and insulators. A basic understanding of the lattice dynamics and phonon structure of these systems are useful in explaining their optical properties and provide useful data for predicting general engineering and research applications.

TABLE OF CONTENTS

1. Introduction and Objectives

The Solid State Spectroscopy laboratory has considerable experience
and expertise in the investigation of the infrared and light scattering proper-
ties of materials. The work has been concentrated on new and prospectively
useful crystals or ceramics in the areas of ferroelectrics, piezo-electrics,
semiconductors, nonlinear materials, electro-optic materials, laser-hosts, etc.
The investigation of the perovskites and the related ilmenites, olivines and
crystobalites may also be advantageous in the identification of the presence
of these materials in igneous rocks which have been discovered on the lunar
surface from the results of the first two Apollo flights.

However, the objectives of the present program have been the inves-
tigation of the optical properties and collectively oscillations in materials
and the change in the properties of these materials under extreme environmental
conditions. In this case, temperature has been the main parameter but with the
high pressure facilities now available it was planned to expand this work in
this direction together with the study of the dielectric constant at low fre-
quencies as a function of both temperature and pressure.

2. Experimental Facilities and Data Analysis

The instrumentation available is summarized below.

Infrared equipment

Perkin-Elmer 301. Double-beam. Spectrophotometer

(Range 2.1-200 micron; 4750-50 cm^{-1})[*]

Far infrared Michelson Interferometer. FS-520

(Range 15-500 microns; 670-20 cm^{-1})

Far infrared Michelson Interferometer. FS-720[*]

(Range 25-2000 microns; 400-5 cm^{-1})

[*]Equipment on loan from NASA (ERC).

Instruments equipped with thermocouple, Golay and liquid helium

cooled bolometer detectors

Spectroscopic Attachments:

(1) Sample holders for transmission and reflection studies

over temperature range 1.5-900°K

(2) Variable angle reflectance units, 10°-70° incidence,

reflection and scattering angles

(3) High pressure studies, 0-50 Kbars on powders

(4) Magnetic field dependence, 0-45 Kilogauss

Light scattering equipment (Rayleigh and Raman)

Spex 1401 double monochromator with linear wave number drive

Laser excitation: Spectra-Physics 125. He/Ne (6328Å) $\sim$ 90 mwatts.

Space-Rays Ar^{+} ion (4880Å) 800 mw and 5145Å (800 mw)*, plus

additional lines of less power

Photon counting detection with FW-130 'Star-tracker' photo-

multiplier, shielded

Facilities for forward, back and right angle scattering geometries

Temperature measurements: 1.5-900°K. Pressure measurements

(forward scattering, 0-50 Kbars; right angle, 0-5 Kbars)

Other equipment and facilities

Polishing and cutting equipment

Metallograph

Machine shop facilities for fabricating specially designed

equipment

X-ray unit (Powder and Laue)

Evaporation unit

Preparation room

Dielectric constant studies down to $1.5^{\circ}K$

Computer facilities

A CDC 3300 computer and a PDP-9 computer are available at Northeastern University. The computers are used to perform Fourier transformations to obtain the long-wave infrared spectra. Kramers-Kronig analyses of the reflectivity data are used to obtain conductivities, absorption coefficients, optical constants, n and k and dielectric constants. Classical dispersion analyses are used to obtain frequencies, oscillator strengths and life-time data on both infrared and light scattering spectra.

3. Experimental Activities

3.1 Optical Phonons and Phase Transitions in TℓI

R. P. Lowndes and C. H. Perry

OPTICAL PHONONS AND PHASE TRANSITION IN TℓI

R. P. Lowndes and C. H. Perry

Solid State Spectroscopy Laboratory

Department of Physics

Northeastern University

Boston, Massachusetts 02115

INTRODUCTION

Thallous iodide exists in two definitely well established modifications.[1-5]   Above $445^{\circ}K$ (at .1 bar) it has the CsCl (Pm3m) structure (TℓI-I) and is bright red in color. In the low temperature modification (TℓI-II) it is yellow and possesses a characteristic layer structure. TℓI-II is built of slices of NaCl structure in which each Tℓ^{+} has five nearest I^{-} neighbors at five of the apices of an octahedron. The neighbors of Tℓ^{+} are one I^{-} at 3.36Å, four at 3.49Å, then two at 3.83Å and two at 3.87Å. X-ray measurements at room temperature were made by Helmholz[1] and the structure is concluded to have four molecules in the unit cell and has the space group D_{2h}^{17}-Cmcm.

The transition between the red (I) and yellow (II) forms is slow and red crystals can even be obtained for some time at room temperature. The low temperature phase has a unique structure and from a chemical viewpoint is of interest because of the large polarizability of the Tℓ^{+} ion and the tendency of iodine to form covalent bonds. The CsCl structure with a coordination number of 8 normally represents the most stable dense configuration but the double layered orthorhombic structure of TℓI (II) has a coordination number of 7 and is less dense than the high temperature cubic form. The cubic phase can be obtained by applying hydrostatic pressure to the material and a pressure of approximately 4.8 kbar and $300^{\circ}K$ is sufficient to cause complete transformation.[2]

The unusual properties of the thallous halides in general make the investigation of this material desirable in order to characterize the relationships in the series. The dielectric constant of TℓI has been investigated by Samara[6] as a function of pressure, and the total polarizability per molecule was found to be effectively independent of crystal structure.

Consequently, the change in dielectric constant can be completely explained by the change in density.

The theories of infrared dielectric dispersion, effective charges and anharmonic effects require measurements of the dielectric constant and the lattice phonon frequencies as a function of temperature.

The infrared active lattice vibration of $T\ell I$ at $300^{\circ}K$ and $4^{\circ}K$ have been measured by Jones et al.[7] and by Claudel et al. at room temperature.[8] Raman measurements by Brafman et al.[9] as a function of pressure have been reported on $T\ell I$ in the region of the phase transition. The transition region as a function of pressure obtained from the Raman intensities was similar to that observed by Samara[6] in the dielectric studies.

In this work we report detailed far infrared and Raman investigations of all the lattice vibrational modes at $k \simeq 0$ of $T\ell I$ over a wide temperature range. These studies include the I → II phase transition, and the mode activities in general agree with the group theoretical predictions from the proposed structures in each phase.

EXPERIMENT

The far infrared spectroscopic investigations were recorded on a modified RIIC FS520 Michelson interferometer[10] used in conjunction with both a Golay detector and a liquid-helium cooled Ga-doped germanium bolometer. Normal incidence transmittance studies of thin films of $T\ell I$ were used to obtain directly the $k \simeq 0$ infrared active phonon frequencies, the dielectric dispersion and damping of the spectral profiles. The films, < 1 micron thick, were evaporated onto crystal quartz and polyethylene substrates. Only the crystal quartz substrates were used at temperatures above $300^{\circ}K$. The frequency

of the lattice vibration at room temperature and below for the films on poly-
ethylene and quartz substrates were in agreement at the same temperature within
the experimental error of the measurements. The films in the TℓI-I phase
could be supercooled to room temperature and only reverted to the yellow form
when the instrument was returned to atmospheric pressure.

Reflection measurements were made on the polycrystalline material
grown using Bridgeman techniques. Samples approximately 10 x 10 mm^2 were
investigated at an angle of incidence of < 10° and the reflectivities were
compared with a freshly aluminized mirror. At high temperatures the poly-
crystalline sample (reflection) and the film on a quartz substrate (trans-
mission) were attached to a heater block. A variable temperature Air Products
Hydrogen Cryotip with appropriate holders was used in the low temperature
investigations together with a conventional fixed temperature cryostat. Back-
ground spectra of the quartz substrate and the mirror were taken at the same
respective temperatures as the samples to obtain the correct transmittance or
reflectance spectra. The temperature of the samples were again monitored
with thermocouples. Attempts to measure the far infrared transmittance or
reflectance at temperatures above 500°K resulted in the films subliming in
the evacuated interferometer.

The Raman spectra were recorded on both a Cary model 81 spectrometer
and a Spex 1400 spectrometer using 6328Å He-Ne excitation. A right angle
scattering geometry was used for powders (in a melting point tube), single
crystals and polycrystalline material.

The detailed studies of the temperature dependence of the Raman
spectra were achieved using the Cryotip refrigeration unit (300 - 20°K) and
a gas transfer sample holder[11] (down to 5°K). High temperatures were

obtained using a Nichrome heater element. Copper-constantant thermocouples were attached to the sample or holder and used to measure the temperature. Control was achieved to approximately $\pm 1^{\circ}$K.

The Raman scattering experiments on the powder and the poly-crystalline sample were identical apart from the width of the transition. In general, the polycrystalline material was completely transformed into the CsCl phase at $\sim 170^{\circ}$C, but on cooling it returned to the orthorhombic modification at 120°C. The transition of the powder in the melting point tube occurred both on heating and cooling within about 10° of the transition temperature of 170°C $(445^{\circ}$K$)$.

Single crystals of thallous iodide were obtained by slowly cooling a solution of the salt saturated at 100°C. Needle-like crystals were formed and according to Helmholz, X-ray measurements indicated that needles grown in this manner were monoclinic and were possibly another modification. However, the Raman spectra of these needles were identical with the powder and the polycrystalline samples. Polarized studies were fruitless and no identification of the symmetric or the antisymmetric modes could be obtained. Considerable birefringence was observed in all the needles under a polarizing microscope and twinning occurred about the 'c' axis??

Both the infrared reflectance and the Raman results of the poly-crystalline material showed that the transition was about 50° wide. The infrared transmission results indicate that the transition region consisted of a mixture of the two phases.

EXPERIMENTAL RESULTS

The Raman spectra of the polycrystalline material is shown in Fig. 1 as a function of temperature. Six bands are clearly observed at low temperatures. The half-widths of the bands increase only slightly as the temperature is raised but the relative intensities of the bands as shown in Fig. 2 are seen to increase as the transition region is approached from below and then decrease as the transformation to the CsCl phase is completed. The reverse procedure is observed on cooling and there is no obvious indication of hysteresis in the Raman spectra apart from the transition region. This is in contrast to the pressure dependent results of Brafman et al.[9] who observe a slight lowering of the intensity as the critical pressure is approached and then a dramatic drop in the intensity at 4.7 kbar. On lowering the pressure, formation of the orthorhombic phase gradually occurs with a slightly less dramatic rise in the intensity of the Raman spectra at 1 kbar.

The optical band gap to some extent influences the Raman intensities in both types of measurement and the form of the sample (solid, needle, powder, thin film, etc.) obviously imposes considerable effects on the width and hysteresis of the transition in both the pressure and temperature domain. Consequently, it is not surprising that the two types of measurement show dissimilar intensity variations.

Above the transition only a very weak second order Raman spectrum is observed with a small side band at ~ 40 cm^{-1}. This shoulder has been interpreted to be probably 2TA(X) and/or LA-TA(X) similar to our results for the other thallous halides[12] and those obtained by Krausman for TℓBr.[13] The frequency dependence with temperature of the Raman bands and also the one infrared band have been obtained. Several thin film transmission data have

been plotted and indicate the large change in frequency of the transverse optic mode at $450^{\circ}K$ and the obvious mixture of the two phases in the transition region present in a thin film.

The infrared reflectance data was analyzed with a Kramers-Kronig analysis to yield dielectric functions $\sigma = \epsilon''\omega$ and $\eta = \epsilon''/\omega$ and typical reflectance, σ and η curves at selected temperatures have been obtained. Peaks in σ and η provided values of the transverse and longitudinal optical mode frequencies respectively and a more detailed plots of the transverse and longitudinal mode frequencies and associated damping constants yield their dependence as a function of temperature. Supercooling of the thin film in the red modification can be seen down to room temperature. Below $450^{\circ}K$ the stability of one phase over another depends on many factors and any form of shock or disturbance immediately renders the orthorhombic form.

The Raman results at room temperature are similar to those obtained by Brafman et al.[9] (except only five bands were observed by these researchers). The infrared data again at room temperature compares favorably with that obtained earlier by Jones et al.[7] on thin films. The reflectance spectra in the low frequency region by Clandel et al.[8] is slightly different from our results.

DISCUSSION

The crystal structure in the cubic phase is CsCl (O_h^1 Pm3m) with $2F_{1u}$ modes, one of which is the infrared active lattice reststrahlen mode and the other corresponds to the acoustic branch. The F_{1u} undergoes a further splitting due to the long range Coulomb forces associated with lattice ionicity and results in 2TO + 1LO modes where TO and LO refer respectively to transverse

optic and longitudinate optic phonons. No first order Raman spectra are allowed and the results are in agreement as shown in Figs. 1-5.

In the low temperature modification with 4 molecules per unit cell, Helmholz[1] proposed the following space groups: C_{2v}^{12}; C_{2v}^{16} and D_{2h}^{17}. The first two possess no center of inversion which imply all modes would be simultaneously infrared and Raman active. Experimentally this is not observed and the space group D_{2h}^{17} (Cmcm) predicts the following modes $2A_g + 2B_{2g} + 2B_{3g} + 2A_{1u} + 2A_{2u} + 2A_{3u}$ of which $1A_{1u} + 1A_{2u} + 1A_{3u}$ are acoustic modes corresponding to the x, y, z crystallographic directions.

The optical phonons in this orthorhombic form that are first order Raman active have the following polarizability tensors, α associated with each of the modes.

$$\alpha[A_g]\begin{pmatrix} a & & \\ & a & \\ & & b \end{pmatrix} ; \quad \alpha_{B_{2g}}\begin{pmatrix} & & e \\ & & \\ e & & \end{pmatrix} ; \quad \alpha_{B_{3g}}\begin{pmatrix} & & f \\ & f & \\ & & \end{pmatrix} .$$

The least one might expect from a right angle scattering geometry with a suitably oriented crystal would be the likelihood of distinguishing between the symmetric A_g and the antisymmetric B_{2g} and B_{3g} modes. However, due to obviously twinned crystals, this measurement was not possible but six modes in agreement with the group theoretical predictions were observed (see Fig. 1).

In the infrared, only one relatively narrow line was observed instead of the predicted three bands corresponding to the three crystallographic directions. It has been assumed that the infrared active modes are essentially degenerate and anharmonic effects must be smaller than its high temperature form or its TℓCℓ and TℓBr counterparts as the line width is quite narrow. As far as this infrared active vibrational mode is concerned the

lattice is essentially isotropic with a coordination number of 7 instead of 8 as in the CsCl modification.

Samara's dielectric data[6] are in agreement with this result as his powder and 'crystal' results essentially agreed and no obvious anisotropies in the static dielectric constant were observed.

ACKNOWLEDGMENTS

REFERENCES

1. L. Helmholz, Z. Krist. **95**, 129 (1936).

2. G. A. Samara, L. C. Walters and D. A. Northrop, J. Phys. Chem. Solids **28**, 1875 (1967).

3. J. C. Zahner and H. G. Drickamer, J. Phys. Chem. Solids **11**, 92 (1959).

4. R. S. Bradley, J. D. Grace, and D. C. Munro, Z. Krist. **120**, 349 (1964).

5. E. Perez-Albuerne and H. G. Drickamer, J. Chem. Phys. **43**, 1381 (1965).

6. G. A. Samara, Phys. Rev. **165**, 959 (1968).

7. G. O. Jones, D. H. Martin, P. A. Mawer and C. H. Perry, Proc. Roy. Soc. **A261**, 10 (1961).

8. J. Claudel, A. Hadni, P. Strimer and P. Vergnat, J. Phys. Chem. Solids **29**, 1539 (1968).

9. O. Brafman, S. S. Mitra, R. K. Crawford, W. B. Daniels, C. Postmus and J. R. Ferraro, Solid State Comm. **7**, 449 (1969).

10. C. H. Perry, R. Geick and E. F. Young, Applied Optics **5**, 1171 (1966).

11. N. E. Tornberg and C. H. Perry, Applied Optics **9**, 777 (1970).

12. R. P. Lowndes and C. H. Perry (to be published).

13. M. Krauzman, C. R. Acad. Sc. Paris **B268**, 148 (1969).

LIST OF FIGURES

Fig.   1

Fig. 2

INTENSITY (ARBITRARY UNITS)

TEMPERATURE °K

TRANSITION

CUBIC

ORTHORHOMBIC

1
2
6
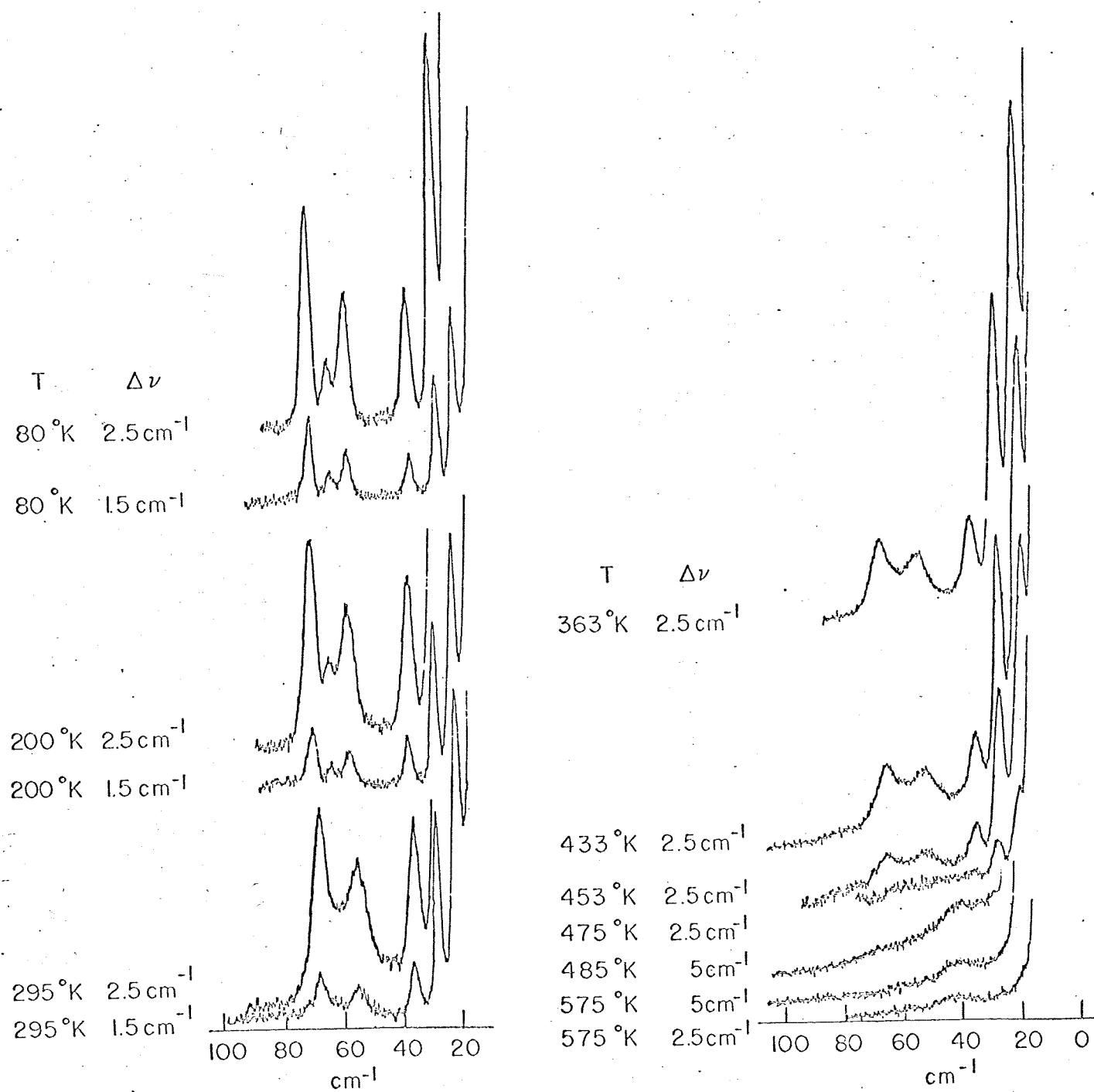4
3
5
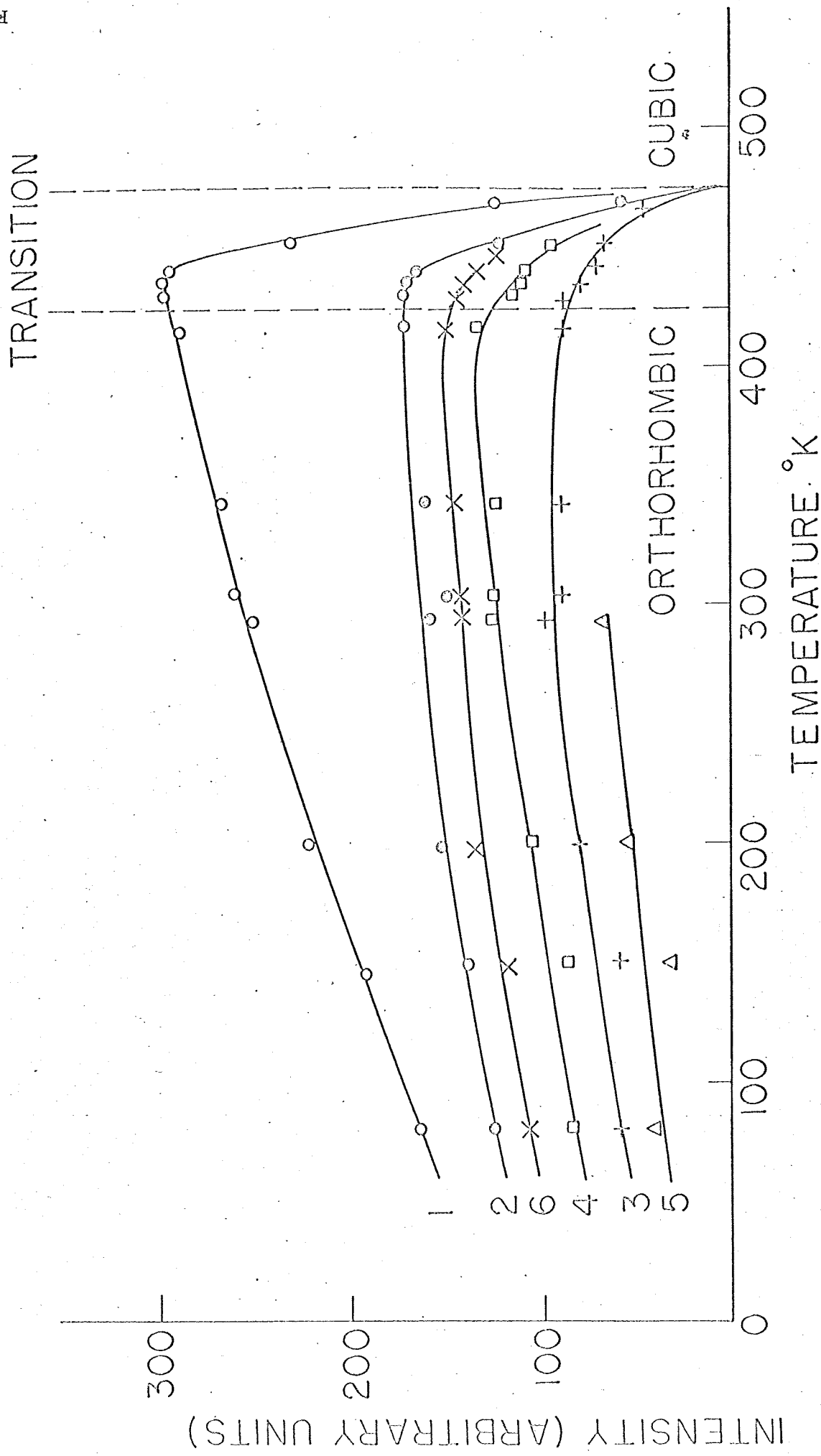
3.2   The Raman Spectrum of SbSI

C. H. Perry and D. K. Agrawal

The Raman Spectrum of Ferroelectric SbSI

C. H. Perry and D. K. Agrawal

Solid State Spectroscopy Laboratory

Department of Physics

Northeastern University

Boston, Massachusetts 02115

Abstract

The polarized Raman spectrum of SbSI has been studied in both the paraelectric and ferroelectric phases. The frequencies and symmetries of most of the Raman active phonons in the paraelectric phase have been determined. A strongly temperature dependent 'A' mode has been observed in the ferroelectric phase which completely accounts for the temperature dependence of the dielectric constant along the ferroelectric axis.

Introduction

Antimony sulpho-iodide (SbSI) is a ferroelectric material with a Curie temperature (T_c) of about $288^\circ K$.[1-4] Above T_c it has an orthorhombic structure with the space group D_{2h}^{16} (Pnam) with lattice parameters a = 8.52Å, b = 10.13Å and c = 4.08Å.[5-7] The static dielectric constant follows Curie Weiss law behavior[7-10] parallel to the 'c' axis and rises to about 5×10^3 at T_c. A sharp decrease is observed as the temperature is lowered through the transition into the ferroelectric phase[7,9] (space group C_{2v}^9 (Pna2$_1$)).[6] Both phases have four formula units per unit cell.

SbSI is a photoconductor with maximum sensitivity at 6300-6400Å.[2,3;11] Below T_c it has been shown that with reference to the iodine atoms the Sb and S atoms are displaced along the 'c' axis by 0.20Å and 0.05Å, respectively.[6] This indicates that the phase transition should be of the displacive type.[12]

In the interpretation of the infrared transmission studies of SbSI powder, Blinc et al.[13] suggest the application of a simplified structure having only two SbSI units and the symmetry change C_{2h}^2 (P2$_1$/m) → C_2^2 (P2$_1$). In this work polarized Raman measurements have been made in both phases. The number and symmetries of the modes observed are substantially in agreement with the simplified structure. In the ferroelectric phase a low frequency temperature dependent mode is observed which shifts towards the Rayleigh line as the transition is approached from below.

Mode Symmetry

In the simplified structure the unit cell now has six atoms with fifteen optical modes and three acoustical modes. In the paraelectric phase there are nine Raman active modes, six of these belonging to A_g and three to

B_g irreducible representation of the point symmetry group C_{2h} of the crystal. In the ferroelectric phase all the fifteen modes are Raman active, eight belonging to A and seven to B symmetry species of C_2.

The corresponding Raman tensors are

$$\alpha(A_g, A) = \begin{pmatrix} a & d & 0 \\ d & b & 0 \\ 0 & 0 & c \end{pmatrix} \quad ; \quad \alpha(B_g, B) = \begin{pmatrix} 0 & 0 & e \\ 0 & 0 & f \\ e & f & 0 \end{pmatrix}.$$

Experiment

The materials used in the present investigations were thin needles (about 1 mm^2 cross section); with the 'c' axis being the needle axis. The crystals were grown from the vapor phase[14] and the growth faces were perpendicular to the [100] and [010] directions. No attempt was made to positively identify the 'a' and 'b' axes as only relatively minor intensity changes were observed by interchanging the designated 'x' and 'y' directions.

The Raman spectra were recorded using an 80 m-watt Spectra-Physics Model 125 He-Ne laser, Spex double monochromator and photoelectron counting detection. An oblique angle 'reflectance' geometry was used and the resolution was normally $\sim$ 2 cm^{-1}. Temperature control both above and below room temperature was achieved with a variable temperature continuous gas transfer cryostat with quartz windows[15]. The temperature was monitored by a copper-constantan thermocouple mounted on the small bracket holding the crystal.

The α_{zz} polarizability tensor component was measured with the crystal 'c' axis along the 'z' direction, the incident laser beam traveling in the 'x' direction and the scattered light collected in the 'y' direction. Both incident and scattered radiation was polarized and analyzed respectively

in the z direction providing a unique measurement of the α_{ZZ} component. The Raman scattering geometry was essentially $\bar{Y}(ZZ)Y$ as the incident beam is traveling approximately in the $\bar{Y}$ in the crystal due to its high refractive index $(\sim 3 - 5)$[16] even though the laser beam outside is more nearly along the 'x' direction. Similarly the spectra corresponding to the α_{XX}, α_{XZ} components were determined.

Results

Figure 1 shows the spectra in the paraelectric phase at $300°K$ for $\bar{Y}(ZZ)Y$, $\bar{Y}(XX)Y$ and $\bar{Y}(XZ)Y$. The assignment of the Raman active phonon frequencies to their respective symmetry types is summarized in Table I. $6 A_g$ and $2 B_g$ modes are observed in close agreement with theoretical predictions.

The temperature dependent Raman spectrum for $\bar{Y}(ZZ)Y$ in the ferroelectric phase is shown in Fig. 2. A marked increase in intensity is observed on cooling from T_c $°K$ to $\sim 240°K$. Further cooling to $100°K$ results in a decrease by about a factor of 2. These intensity changes may be due to the change in optical absorption edge ($E_g = 1.95$ eV for $E//c$ at room temperature[2,3,11]). The edge increases with decreasing temperature at an average rate of $\cong 1.5 \times 10^{-3}$ eV/$°K$.[2] Lowering the temperature therefore raises E_g above the exciting laser energy of 1.96 eV, at $\sim 18°C$. The slight change in the lattice parameters along the c-axis in the ferroelectric phase[7,9] might cause the Raman tensor components to be temperature dependent. The decrease in intensity from $\sim 240°K$ lower temperature may be accounted for by the anomalous decrease in the spontaneous polarization P_s as observed by Pandey[17] in polycrystalline SbSI due to the ferroelectric domain structure at low temperatures.

Some of the infrared active modes observed by Blinc et al.[13] below T_c are now Raman active and are observed in the spectrum at 253, 167 and 70 cm^{-1}. The majority of lines, however, are relatively temperature independent except for the band at 50 cm^{-1} at $100^o K$ (see Fig. 2), which moves to lower frequency as T approaches T_c from below. The temperature dependence of this mode in the ferroelectric phase is shown in Fig. 3. Application of Cochran's theory for displacive ferroelectrics[18] ($\epsilon_o(T) \alpha \frac{1}{\omega^2(T)}$) to non-cubic crystals can be applied to the generalized Lyddane-Sachs-Teller relationship[19]

$$\frac{\epsilon_o(\ell)}{\epsilon_\infty(\ell)} = \prod_i \frac{\omega_{L_i}(\ell)}{\omega_{T_i}(\ell)}$$

where 'ℓ' refer to the 'ℓ' axis in the crystal. The logarithmic differential form of this equation has been derived by Barker[20] and allows measurements of the contributions of phonons to the dielectric constant below T_c.

$$\frac{\Delta\epsilon_o}{\epsilon_o} = \frac{2\Delta\omega_{L_1}}{\omega_{L_1}} + \frac{2\Delta\omega_{L_2}}{\omega_{L_2}} + \ldots - \frac{2\Delta\omega_{T_1}}{\omega_{T_1}} - \frac{2\Delta\omega_{T_2}}{\omega_{T_2}} - \ldots \quad .$$

In Fig. 4, $\frac{\Delta\epsilon_o}{\epsilon_o}$ as a function of temperature for $T < T_c$ is shown from the dielectric data of Masuda et al.[7] and Hamano et al.[9] measured along the ferroelectric 'c' axis.

Only the transverse mode in the 'z' (c) direction shown in Fig. 3 has any marked temperature dependence and the quantity $\frac{-2\Delta\omega_{T_1}}{\omega_{T_1}}$ derived from Fig. 3 is also shown in Fig. 4.

-7-

The agreement of the two curves suggests that this mode completely accounts for the temperature dependence of the dielectric constant in the ferroelectric phase.

Summary

The symmetries of the group theoretically allowed modes for the simplified structures proposed by Blinc et al.[13] are in good agreement with these Raman studies of single crystals in both the paraelectric and ferroelectric phases. The frequency dependence of the transverse A mode in Fig. 3 shows a softening as $T \rightarrow T_c$ from below and it completely determines the temperature dependence of the static dielectric constant along the 'c' axis in the ferroelectric phase. This mode can be associated with the 'soft' mode present in the paraelectric phase observed as the peak in ϵ'' by Grigas and Karpus[21] at ~ 0.5 cm^{-1} at $308°K$ and the results demonstrate that SbSI is a displacive ferroelectric similar to the perovskites.

It is unlikely that the 'soft' mode in paraelectric phase can be observed directly in the far infrared reflectance spectrum but preliminary measurements in this laboratory indicate that an extremely low frequency A_u mode is present. The complete infrared mode polarizations and corresponding symmetries are being analyzed and these results will be reported elsewhere.

Acknowledgments

References

1. Nitsche, R. and Merz, W. J., J. Phys. Chem. Solids 13, 154 (1960).

2. Kern, R., J. Phys. Chem. Solids 23, 249 (1962).

3. Harbeke, G., J. Phys. Chem. Solids 24, 957 (1963).

4. Fatuzzo, E., Harbeke, G., Merz, W. J., Nitsche, R., Roetschi, H., and
    Ruppel, W., Phys. Rev. 127, 2036 (1962).

5. Dönges, E., Z. Anorg. Cheme. 263, 112 (1950).

6. Kikuchi, A., Oka, Y., and Sawaguchi, E., J. Phys. Soc. Jap. 23, 337
    (1967).

7. Masuda, Y., Sakata, K., Hasegawa, S., Ohara, G., Wada, M., and
    Nishizawa, M., Jap. J. App. Phys. 8, 692 (1969).

8. Nakamura, E., Mitsui, T., and Furuichi, J., J. Phys. Soc. (Japan) 18,
    1477 (1963).

9. Hamano, K., Nakamura, T., Ishibashi, Y., and Ooyane, T., J. of Phys.
    Soc. (Japan) 20, 1886 (1965).

10. Mori, T., and Tamura, H., J. Phys. Soc. (Japan) 19, 1247 (1964).

11. Sasaki, Y., Japan J. Appl. Phys. 3, 558 (1964).

12. Takama, T., and Mitsui, T., J. Phys. Soc. (Japan) 23, 331 (1967).

13. Blinc, R., Mali, M., and Novak, A., Solid State Communications 6, 327
    (1968).

14. Molnar, B., Johannes, R., and Haas, W., Bull. Am. Phys. Soc. 10, 109
    (1965).

15. Tornberg, N. E., and Perry, C. H. (submitted to Applied Optics).

16. Johannes, R., and Haas, W., Applied Optics 6, 1059 (1967).

17. Pandey, R. K., J. of Phys. Soc. (Japan) 27, 633 (1969).

18. Cochran, W., Phys. Rev. Lett. 3, 412 (1959).

19. Cochran, W., and Cowley, R. A., J. Phys. Chem. Solids 23, 447 (1962).

20. Barker, A. S., Jr., Ferroelectricity, edited by F. Weller (Elsevier Publishing Co., Amsterdam 1967), p. 238.

21. Grigas, I. P., and Karpus, A. S., Sov. Phys. Solid State 9, 2270 (1968).

Table I

Assignment of the Raman Active Phonon Modes in the Paraelectric Phase

Raman Active Phonon Frequencies (cm^{-1})	Symmetry Species	Raman Tensor Components
51	A_g	α_{XX}
66	A_g	α_{XX}
107	A_g	α_{XX}, α_{ZZ}
137	A_g	α_{XX}, α_{ZZ}
149	A_g	α_{XX}
319	A_g	α_{XX}
37	B_g	α_{XZ}
212	B_g	α_{XZ}
-	B_g	α_{XZ}

-11-

List of Figures

SbSI $\Delta\nu \simeq 2\,cm^{-1}$ 100°K $\bar{Y}(ZZ)Y$

3.3 Far Infrared Stark and Zeeman Splittings of Er^{3+}

in the Lanthanide Fluorides

J. F. Parrish, C. H. Perry and R. P. Lowndes

Far Infrared Stark and Zeeman Splittings

of Er^{3+} in the Lanthanide Fluorides[*]

J. F. Parrish[**], C. H. Perry and R. P. Lowndes

Research Laboratory of Electronics, Massachusetts
Institute of Technology, Cambridge, Massachusetts 02139

and

Solid State Spectroscopy Laboratory, Department
of Physics, Northeastern University, Boston, Massachusetts 02115

[**] Present address: Department of Physics, Shell Development
                       Company, P.O. Box 481, Houston, Texas 77001.

-2-

Abstract

The first excited Stark level of the Er^{3+} ion in LaF_3, CeF_3, PrF_3 and NdF_3 has been observed near 55 cm^{-1}. Zeeman splitting reveals at least two magnetically distinguishable Er^{3+} sites and confirms the electronic nature of the transition.

The first excited Stark level of the $^4I_{15/2}$ ground multiplet of the Er^{3+} ($4f^{11}$) ion in LaF_3 is expected to be approximately 52 cm^{-1} above the ground level.[1,2] A far infrared active transition between these two Stark levels has been observed directly in the polarized transmittance spectra of oriented, single crystals of LaF_3, CeF_3, PrF_3 and NdF_3 doped with one mole per cent Er^{3+}. The measurements were obtained on $\sim$ 1 mm. thick samples cooled to 7 $\pm$ 2°K using a far infrared Michelson interferometer and a liquid helium cooled detector. A single crystal of LaF_3 (1% Er^{3+}) mounted in a light pipe and submerged in liquid helium at 1.33 $\pm$ 0.03°K was used for the Zeeman study. The infrared radiation propagated parallel to the applied magnetic field and made an angle of 45° with respect to the optic axis of the crystal. The light pipe-sample holder geometry precluded any meaningful polarized Zeeman studies.

The polarized transmission results are summarized in Table 1. The experimental measurements indicate that the Er^{3+} transition is unpolarized but possesses a characteristic anisotropy such that the σ-polarization is approximately fifty percent stronger than the π-polarization.

The transition could not be observed clearly in the π-polarization of PrF_3 because it was obscured by the strong, almost π-polarized electronic transition at 66 cm^{-1} of the Pr^{3+} ions in PrF_3[3,4]. Note that the frequency of the Er^{3+} transition increases by over 10% for a decrease in the lattice constants of about 1.5%, whereas the 45 cm^{-1} Nd^{3+} transition frequency shifts by only 3% in the same materials.[3]

In a magnetic field of 20 kilogauss, the LaF_3:Er^{3+} absorption line at 52 cm^{-1} broadens into a band extending from 52.5 to 58.5 cm^{-1}. With increasing magnetic field, this broad band separates into several distinct lines as shown in Fig. 1. Solid lines connect peaks of four Zeeman

-4-

transitions and two broken lines indicate possible fifth and sixth Zeeman transitions. Individual peaks are 0.1 to 0.2 as strong as the zero field line.

Several Zeeman levels can be resolved because the g-tensor of the ground state, Stark level of Er^{3+} in LaF_3 is strongly anisotropic.[5] Nevertheless, only significant upper and lower bounds of the g-tensor can be stated as a unique assignment would require measurements in at least three different orientations. The results indicate that there are at least two and probably three magnetically distinguishable erbium sites in the tysonite lattice. The maximum value of g for the excited Stark level in this orientation lies between 1.8 and 7.5 ± 0.5 and the corresponding minimum value lies between 1.3 and 3.5 ± 0.5.

Table 1

Er^{3+} electronic transition in LaF_3, CeF_3, PrF_3 and NdF_3.

Host lattice		LaF_3	CeF_3	PrF_3	NdF_3
Frequency (cm^{-1})		52.0 ± 0.5	53.5 ± 0.5	56.7 ± 0.5	57.7 ± 0.5
Half-width	π	< 1.5	~ 2.5	< 1.5	< 2.0
(cm^{-1})	σ	< 1.5	~ 3.0	< 1.5	< 2.0
Peak absorption (cm^{-1})	π	5.2	10.8	⩽ 40	12.4
	σ	8.4	15.9	10.0	18.2

-6-

References

1. W. F. Krupke and J. B. Gruber, J. Chem. Phys. $\underline{41}$, 1225 (1964).

2. W. F. Krupke and J. B. Gruber, J. Chem. Phys. $\underline{39}$, 1024 (1963).

3. J. F. Parrish, R. P. Lowndes and C. H. Perry, Phys. Letters $\underline{29A}$, 270 (1969)

4. R. P. Lowndes, J. F. Parrish and C. H. Perry, Phys. Rev. $\underline{182}$, 913 (1969).

5. J. M. Baker and R. S. Rubins, Proc. Phys. Soc. $\underline{78}$, 1353 (1961).

Figure Caption

Fig. 1   Zeeman splitting of Er^{3+} in LaF_3.

Figure axes: MAGNETIC FIELD (KILOGAUSS), WAVE NUMBER (CM⁻¹)

Δg=6.7±0.2

Δg=4.9±0.2

Δg=3.3±0.2

Δg=1.9±0.3

Δg=0.5±0.4

Δg=-0.8±0.4
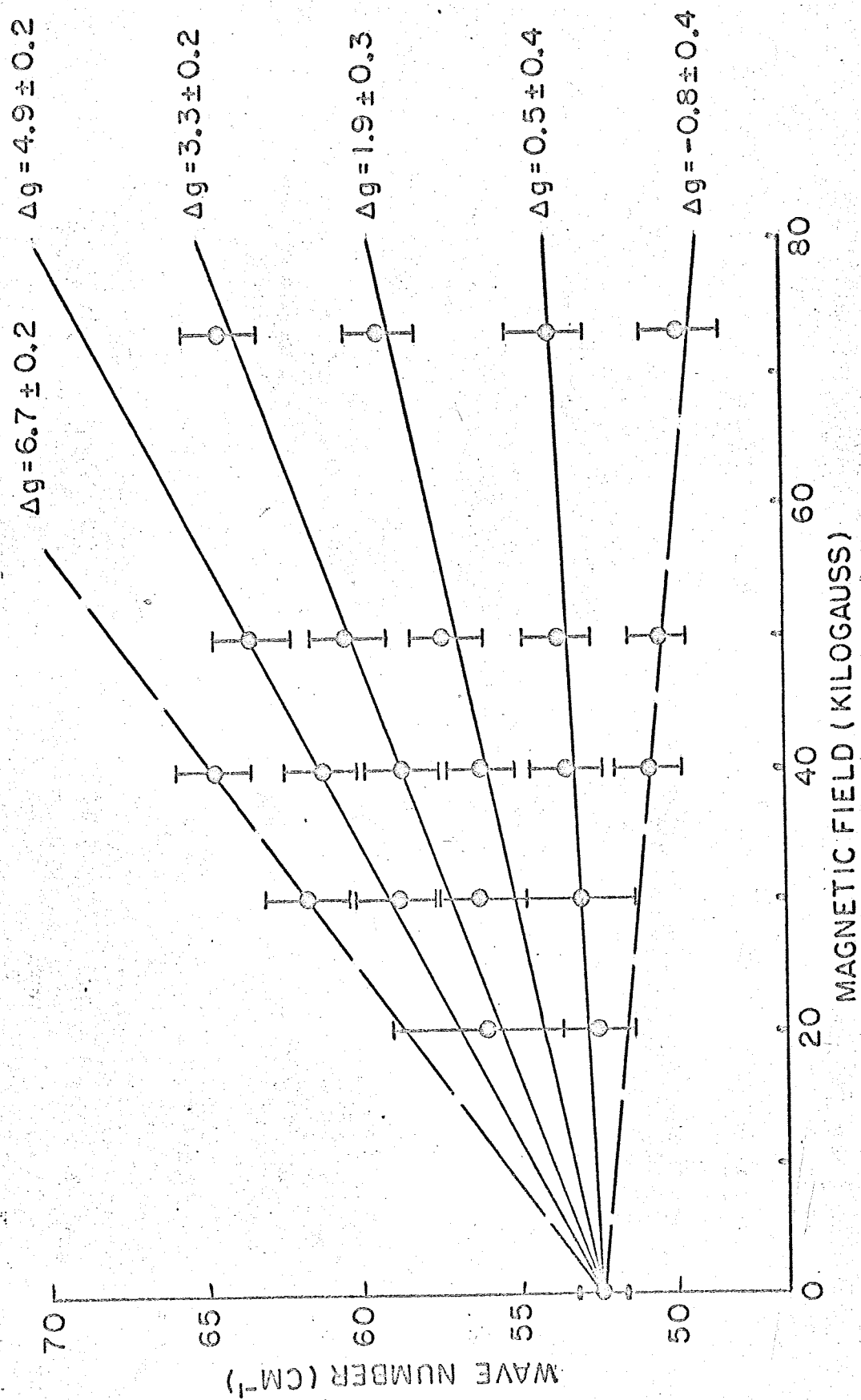
3.4 A Variable Temperature (8-400$^\mathrm{o}$K) Gas Transfer Cell

for Solid State Spectroscopy

N. E. Tornberg and C. H. Perry

A Variable Temperature (8-400°K) Gas Transfer Cell

for Solid State Spectroscopy

N. E. Tornberg and C. H. Perry
Research Laboratory of Electronics and Spectroscopy Laboratory,
Massachusetts Institute of Technology,
Cambridge, Massachusetts 02139

and

Solid State Spectroscopy Laboratory,
Department of Physics, Northeastern University,
Boston, Massachusetts 02115

INTRODUCTION

Many intensive studies that involve Raman spectroscopy as an observational tool also require the control and variation of temperature. A common spectrophotometer used in such work is the Cary model 81 with He-Ne laser excitation. In that instrument, the laser beam is directed at the sample from overhead, rendering the use of usual dewar design impractical if not impossible. Although long term precision control of the temperatures attained was not deemed necessary in the authors' work, it was desired that the entire range from 300° to somewhat below 20°K be attainable without changing critical sample illumination geometries. Also, it was considered worthwhile that sample changing be quick and convenient and thus that temperature cycling be fairly rapid within the above range. It was felt that the best means of dealing with these requirements and restrictions was through the use of a cell which achieved temperature control by means of precooled or preheated gas directed at a metal block in thermal contact with the substance under study. The design presented here resulted from these considerations.

CELL DESIGN

The cell consists of four principle elements which are shown in Fig. 1. Element I is a modified transfer tube with an expanded outer jacket at the interface with the rest of the system to which an "O" ring seal is effected. About this expanded section is a ring with a longitudinal slot which may be clamped to the jacket by tightening a screw traversing the slot. This ring acts as a stop to hold the end of the transfer tube a predetermined distance from the back of the sample block.

Element II consists, in sequence, of the above-mentioned "0" ring seal assembly, radial vent holes distributed about its circumference to release spent coolant gas, a short section of tube to mate with the "0" ring seal in element III, and a concentric inner tube which supports the copper sample block. The outer tubular section serves as a portion of the outer vacuum jacket and the copper sample block features a $\frac{1}{4}$ x 20 threaded hole on its sample face to accept the actual sample holder. Part way back from the sample block a copper collar is mounted on the tube on which a radiation shield which encloses the sample area may be mounted by a snug force-fit. Electrical leads may be led into the sample area by means of a slot in the collar. This collar, and thus the shield, are cooled by the exiting coolant, which also serves to cool the outer case of the transfer tube. Another slotted ring clamp surrounds the outer concentric tube to establish the longitudinal location of the sample area within the cell.

Element III serves as a mount for a pump-out port and for electrical feedthroughs into the sample area. It also connects the preceding portions of the cell to the tail portion of the vacuum jacekt. This element consists, in sequence, of the "0" ring seal assembly for element II, the electrical feedthrough assembly on a demountable flange and opposite this a pump-out port including a valve to isolate the cell, and an "0" ring seal assembly to join to the tail vacuum jacket.

Element IV is the tail section vacuum jacket. This consists simply of a tube terminated at one end with a rectangular block containing ports, "0" ring seals, and mounting provision for windows of quartz or other material.

-4-

CELL USE

Temperatures up to approximately 130°C could be obtained by replacing the element I (modified transfer tube) with a porcelain tube around which a nichrome heater was wrapped and through which the gas was passed. Since elevated temperatures could be obtained more easily by other means, however, heated air (or nitrogen) was used primarily to warm up an already cold cell if condensation on the sample was to be avoided. Cold gas was obtained in one of two ways. First, nitrogen was passed through a copper coil immersed either in a dry ice-acetone solution or in liquid nitrogen. Second, an approximately 10 ohm wirewound resistor powered by a commercial 25 v, 5 amp variable power supply was used to boil liquid helium. A modified tip on the transfer tube accepted the gas above the liquid, passed it through an outer tube to the tip's end near the bottom of the dewar and hence through an inner tube to the transfer tube proper.

A standard Janis Research Co. flexible transfer tube was used for the helium gas. One end was modified by being shortened and given an expanded jacket as indicated above. The tube used for nitrogen was merely the expanded jacket and short vacuum-insulated tip since the cold temperature bath was commonly placed near the cell and a short piece of insulated hose connected the copper coil in the bath to the cell.

Although the design included provisions for partial temperature control by adjusting the distance from the transfer tube outlet to the back of the sample block, it was found that this did not have a usefully large effect within the range of movement possible ($\sim 2\frac{1}{2}$"). Thus, all temperature control was achieved by controlling gas temperature and flow rate. In Fig. 2 are data representing the average conditions encountered in attempting to

maintain low temperatures with cold helium gas. Convenient control could be obtained in the region 20°-50°K without the shield and 8°-25°K with it. Within these regions temperature could be stabilized within $\pm 0.2^\circ$K for periods of 30 minutes or more. The large copper block damped temperature fluctuation due to variations in gas flow with an estimated time constant of from 2 to 5 minutes, depending on temperature. The radiation shield mounting collar was about 5 3/4" from the sample area and at lower sample temperatures the shield operated at from 60 to 65°K.

At higher temperatures the radiation shield still had some effect. With it installed temperatures from essentially that of liquid nitrogen could be obtained using nitrogen cooled in a bath of the liquid gas; without it, required gas flow was too small for good control at about 120°K.

Using dry ice-acetone as the cooling bath, temperatures from 200°K could be obtained by regulating gas flow alone.

Temperatures above the indicated ranges for helium- or nitrogen-cooled transfers could be easily attained. However, the small gas flow required rendered control somewhat uncertain with the result that long term stabilization to better than $\pm 2^\circ$K could not be obtained. In the case of liquid nitrogen cooling, this could easily be circumvented by a less efficient heat exchanger in the bath or a heater on the transfer tube. For liquid helium cooling, a heater could easily be mounted in the sample area for dynamic heat flow balance at higher temperatures. In both cases, exact temperature control was not required by the authors in the ranges indicated so these modifications were not effected.

In general use, it was found that temperature cycling could be made quite rapid. The transition from 300° to 20°K could be made in about 10 minutes, with the warmup using heated air requiring about the same length of time.

Controlled, slow temperature sweeps were also quite easily accomplished permitting detailed examination of the effects of phase transitions on the spectra.

Mechanically, the cell proved quite convenient to use. The tail jacket was clamped into the sample - illuminating chamber of the spectrometer by a slotted ring mounted on its case. The cell itself was supported by a pair of chain clamps mounted on an optical rail aligned with the optic axis of the Cary spectrometer. This permitted the cell (without tail vacuum jacket) to be quickly extracted from the spectrometer by sliding its mounts along the rail. It would then be very easily returned to its previous configuration. Sample orientation could be accomplished quite easily because of the longitudinal and rotational degrees of freedom. Also, the transfer tube portion could be removed without significantly disturbing the remainder, thus permitting operation over the entire attainable temperature range without attention to optical alignment. The cell could easily be configured for various sample illumination geometries by providing various tail jackets - relatively small pieces to make. Considerable frost could build up about the gas vents but did not prove a problem. Stainless steel was used exclusively except for the copper portions with the result that the cold portions of the case were quite localized due to the poor heat conduction.

FURTHER APPLICATIONS

The success of the cell as specifically applied to studies involving the Cary instrument, along with its small size, light weight, easily changed geometry, and insensitivity to operating position, suggested its usefulness in a wide variety of applications. It was easily adapted for use with the

Spex double monochromater with laser excitation since it could, with a minimum of external support, be mounted vertically on the lid of the sample illuminator supplied as an option with that instrument. Its operation in that configuration did not vary significantly from that described above. Operated vertically, it could also be used as a conventional dewar for liquid nitrogen and warmer baths. The hold time for the small quantity of liquid nitrogen it would contain proved to be approximately 40 minutes, generally adequate for spectroscopic work.

The cell's versatility was extended to infrared investigations by using CsI and polyethylene windows, either on the same tail vacuum jacket or on another. In this configuration it has been used in transmission with Perkin Elmer models 301 and 521 grating instruments, and Beckman models FS 720 and FS 520 Michelson interferometers. With the latter it has also been used in reflection, its quick temperature cycling allowing rapid change between the two, since multiple tail jackets can be mounted at different locations in the sample chamber. The cell also has been used successfully with an evaporator attachment for first obtaining thin films _in situ_ and then, by rotating the cell 90° within the vacuum jacket, taking direct infrared transmission measurements.

This cell has been employed in several solid state spectroscopic investigations, the results of which appear elsewhere in the literature. [1-4]

REFERENCES

1. C. H. Perry and N. E. Tornberg, Phys. Rev., 10 July, 1969 (in print).

2. N. E. Tornberg and C. H. Perry, Solid State Comm. $\underline{6}$, XVI (1968) and in Conference on Light Scattering Spectra of Solids, ed. G. B. Wright (Springer-Verlag, New York, 1969), paper F3, pp. 467, 476.

3. C. H. Perry and R. P. Lowndes, J. Chem. Phys., October (1969) (in print).

4. R. P. Lowndes and C. H. Perry, paper T5, Molecular Spectroscopy Symposium, Ohio State University, Columbus, Ohio, Sept. 2-6, 1969, p. 88.

FIGURE CAPTIONS

Fig. 1   Simplified mechanical drawing of temperature-control cell.

A .   Transfer tube out to supply of refrigerant gas.

B   Omission of 1 3/8" of material

C   Omission of 2" of material

D   Tube out to vacuum feedthroughs on demountable flange

E   Tube out to valve and evacuation line

F   Omission of $4\frac{1}{4}$" of material

1   Helium or nitrogen precooled gas in through center of transfer tube

2   Vacuum space of transfer tube

3   Expanded outer transfer jacket

4   Ring clamp to limit longitudinal motion

5   Coolant gas vent

6   Clamping nut for "0" ring seal

7   "0" ring

8   Shoulder with slightly smaller inner diameter to limit travel of other elements

9   Evacuable space

10   Copper radiation-shield - mounting collar

11   Radiation shield

12   Copper sample block

13   Sample holder

14   Window

Fig. 2   Typical helium flow rates vs. temperatures attained, with and without radiation shield.

HELIUM GAS TRANSFER RATE (LIQUID LITERS/HR) vs TEMPERATURE (°K)

WITH SHIELD
WITHOUT SHIELD
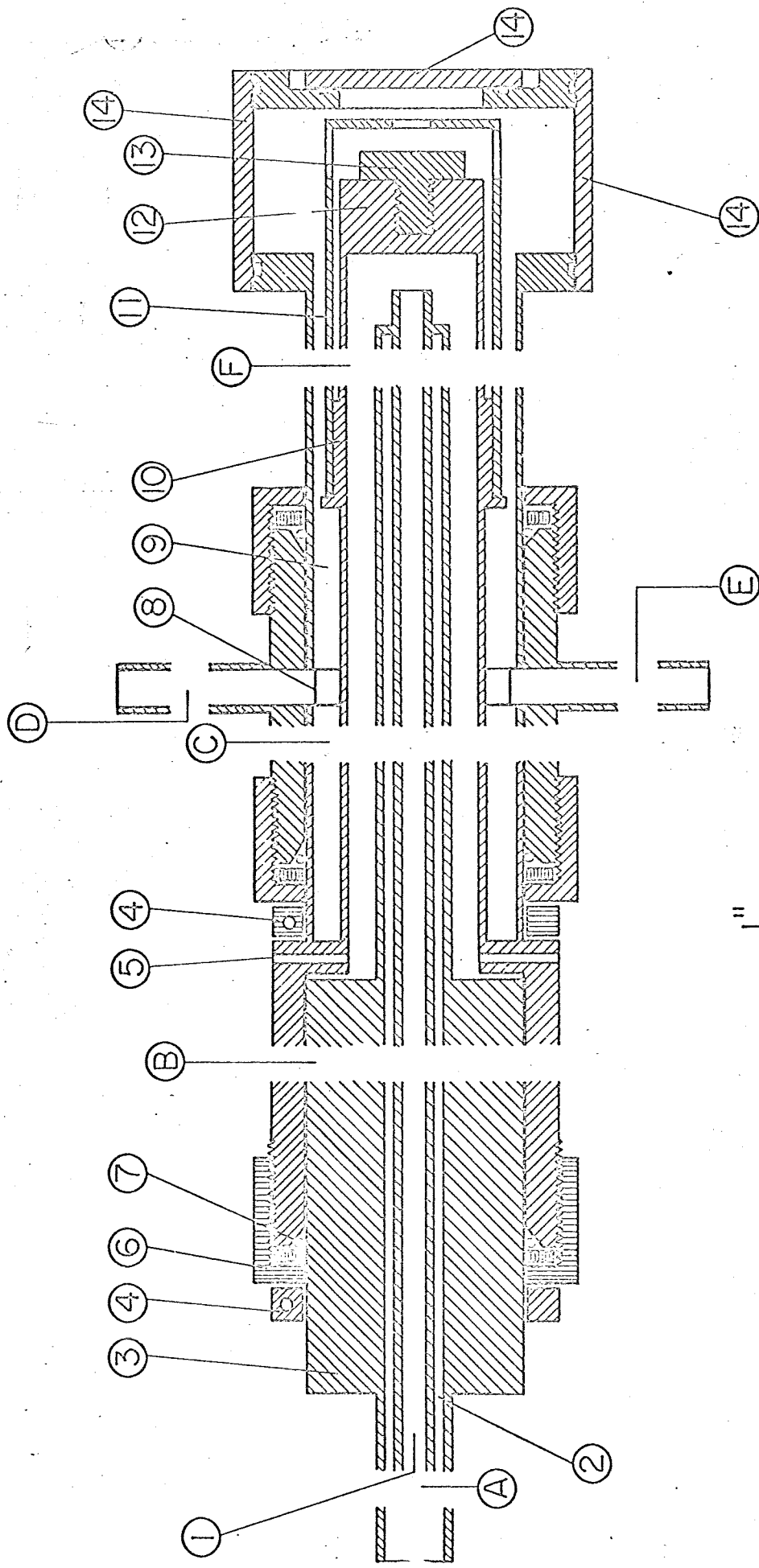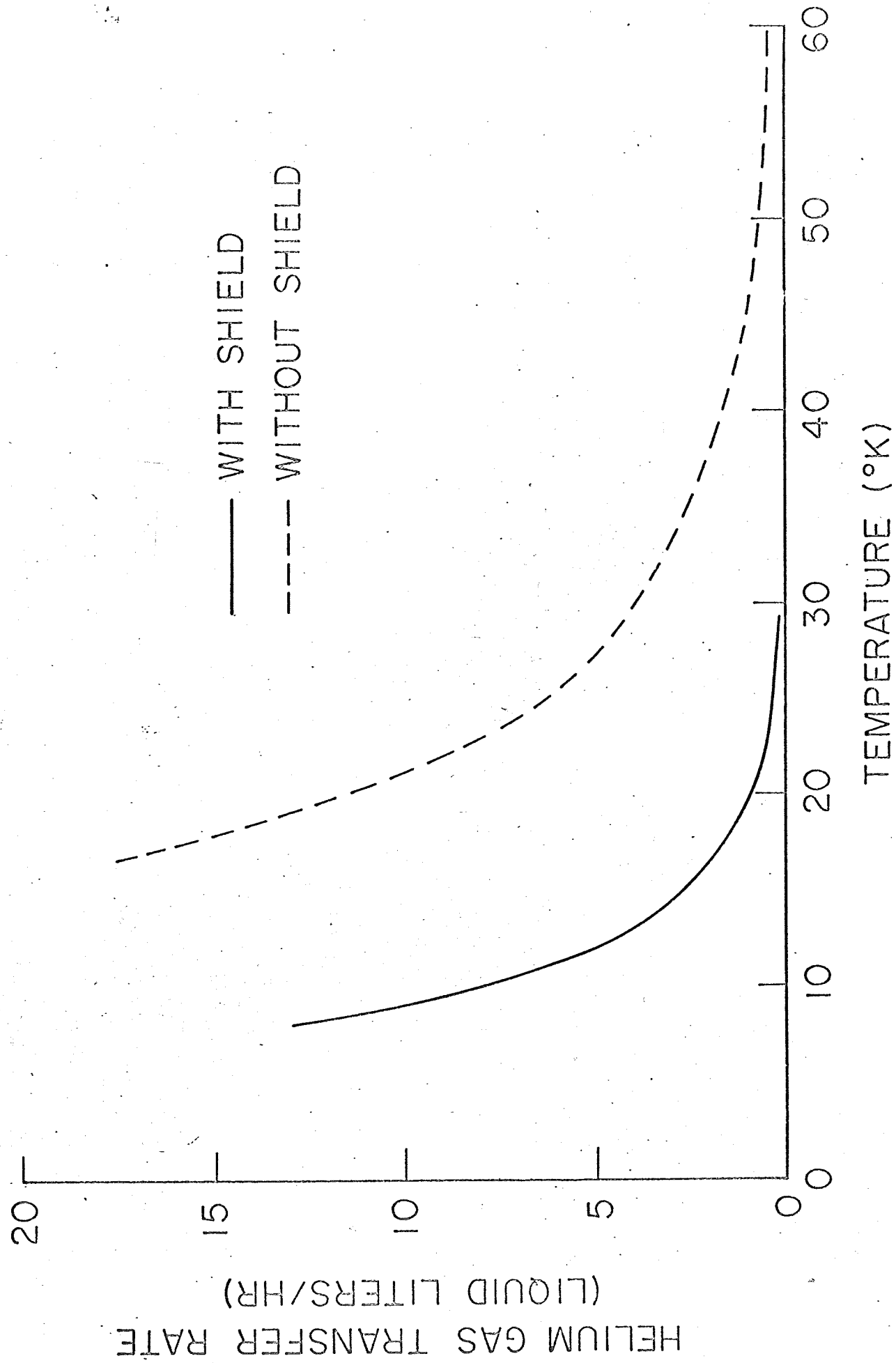
3.5 The Influence of Lattice Anharmonicity on the

Longitudinal Optic Modes of Cubic Ionic Solids

R. P. Lowndes

The Influence of Lattice Anharmonicity on the Longitudinal
Optic Modes of Cubic Ionic Solids

R. P. Lowndes
Spectroscopy Laboratory, Research Laboratory of Electronics [§]
Massachusetts Institute of Technology, Cambridge, Massachusetts

and

Solid State Spectroscopy Laboratory
Physics Department, Northeastern University, Boston, Massachusetts 02115

ABSTRACT

The determination of the $k \approx 0$ longitudinal optic mode frequencies and lifetimes from the dielectric, $\epsilon(\omega)$, and inverse dielectric, $\eta(\omega)$, reponse functions of simple cubic solids is discussed. Experimental results of the temperature dependence, over the range $5°-400°K$, of the $k \approx 0$ LO frequencies and lifetimes of eighteen alkali and thallium halides are given, as determined from Kramers-Kronig analyses of near normal incidence single crystal reflectance data and from small grazing angle reflectance data of thin films on conducting substrates. In addition, the pressure dependence up to 5 kilobars at $290°K$ of the LO frequencies of RbI, CsBr and CsI are reported. At $5°K$ the Lyddane-Sachs-Teller relation holds within $\pm 3\%$ for all the salts, and even at $290°K$ the relation is obeyed within $\pm 10\%$. The temperature and pressure results are used to determine the self-energies and Gruneisen constants for the LO modes. At room temperature the measurements reveal that the self-energies can either enhance or oppose the temperature dependence of the modes arising from thermal expansion. This is interpreted in terms of competing three phonon and four phonon decay and scattering processes.

Note: The pressure work was performed at Queen Mary College, University of London.

1. <u>INTRODUCTION</u>

If the lattice potential energy of a crystal were perfectly harmonic the phonon frequencies would be independent of both temperature and volume. Evidence of the actual anharmonic lattice potential present in real materials like the alkali halides is readily available from a variety of experimental investigations, for instance from the observed temperature[1,2] and volume[3,4] dependence of the frequencies and lifetimes of the $k \approx 0$ transverse optic modes of these salts. The investigations conducted so far have revealed only a small intrinsic temperature dependence of the $k \approx 0$ transverse optic modes compared to their intrinsic volume dependence.[4] To date, few investigations of any kind of the $k \approx 0$ longitudinal optic modes of the alkali halides have been made.[5] In this paper we report on the detailed temperature dependence of the $k \approx 0$ longitudinal modes for some alkali and thallium halides and also on the pressure dependence of these modes for RbI, CsBr and CsI. The results are used to separate those effects of anharmonicity which are explicitly temperature dependent from those which are explicitly volume dependent. The former contributions are discussed in terms of the self-energies of the $k \approx 0$ longitudinal optic modes and the latter contributions are discussed in relation to the Gruneisen constants of these modes.

-3-

2. DETERMINATION OF THE LO FREQUENCIES AND LIFETIMES

Although the transverse nature of electromagnetic waves prohibits their interaction with longitudinal optic phonons in infinite media, Berreman[5] has shown for cubic systems and Lowndes et al.[6] have shown for anisotropic systems that infrared absorption measurements can, for suitable sample-radiation geometries, be used to measure the frequency of $k \approx 0$ longitudinal optic phonons when thin strata (non-infinite) samples are used. We discuss now the significant properties of the dielectric response functions for cubic systems by which a determination of the $k \approx 0$ LO phonon frequencies and lifetimes is achieved from infrared spectroscopic measurements.

For cubic systems the three principal components of the dielectric tensor are degenerate. In the following discussion it is assumed that the applied electromagnetic fields are small compared to the internal crystal fields and hence we may retain only a linear relation between the dielectric displacement, D, and the electric field, E, which may be written either as

$$D(\omega) = \epsilon(\omega)E(\omega) \tag{1}$$

where $\epsilon(\omega)$ is a frequency dependent complex dielectric constant, or as

$$E(\omega) = \eta(\omega)D(\omega) \tag{2}$$

where

$$\eta(\omega) \equiv \frac{1}{\epsilon(\omega)} . \tag{3}$$

The choice of equation depends on the type of vibration under consideration and will be determined by whether $D(\omega)$ or $E(\omega)$ drives the system. In dealing with long wavelength transverse optic waves the electric field $E(\omega)$ drives the system and hence the use of the dielectric response function, $\epsilon(\omega)$, in Eq. (1) is the more appropriate response function in this case. In dealing with long wavelength longitudinal optic modes it is the dielectric displacement, $D(\omega)$, which

drives the system and the inverse dielectric response function, $\eta(\omega)$, is now

more appropriate.[7]

Both $\epsilon(\omega)$ and $\eta(\omega)$ will in general be complex and for $\epsilon(\omega)$ and $\eta(\omega)$

to follow causal behavior requires that $\epsilon(\omega) = -\epsilon^*(\omega)$ and $\eta(\omega) = -\eta^*(\omega)$, where

the asterisk indicates the complex conjugate. Because of causality the poles

and zeros of $\epsilon(\omega)$ and $\eta(\omega)$ will be either above the real axis or below it[8]

depending on which sign convention is used to describe time periodic functions.

Since the dielectric constant for the compounds considered here is a scalar

quantity, causality further requires that the poles and zeros of $\epsilon(\omega)$ and $\eta(\omega)$

be symmetrically distributed about the imaginary axis of the ω plane[8] (this

would also be true for a second-rank tensor dielectric response function). It

is clear that a pole of $\epsilon(\omega)$ and a zero of $\eta(\omega)$ will occur whenever a frequency

ω_T occurs for which $E(\omega_T) = 0$ and $D(\omega_T) \neq 0$, that is for a transverse optic

frequency; similarly a zero of $\epsilon(\omega)$ and a pole of $\eta(\omega)$ will occur for a fre-

quency ω_L at which $E(\omega_L) \neq 0$ and $D(\omega_L) = 0$, that is at a longitudinal optic

frequency.

We are primarily concerned here with the response function $\eta(\omega)$. The

most general form for $\eta(\omega)$ for a system of N oscillators may be written as[9]

$$\eta(\omega) = \prod_{j=1}^{N} \eta_\infty \frac{(\omega - \omega_{Zj})(\omega - (-\omega_{Zj}^*))}{(\omega - \omega_{Pj})(\omega - (-\omega_{Pj}^*))} \tag{4}$$

where ω is the applied field frequency and ω_Z and ω_P represent, respectively,

the complex frequencies of zero's and poles in $\eta(\omega)$; η_∞ is a constant used to

collectively describe the poles and zero's in $\eta(\omega)$ due to intrinsic electronic

transitions and is defined as $\eta_\infty = \frac{1}{\epsilon_\infty}$, where ϵ_∞ is the high frequency dielec-

tric constant. Because of the consequences of anharmonic interactions in real

crystals the locations of the transverse and longitudinal optic mode frequencies

and their associated damping can be defined in a somewhat arbitrary manner and

we do so here in the following way:

$$\omega_{Tj}^2 = (\omega_{Zj}')^2 + (\omega_{Zj}'')^2 \qquad (5a)$$

$$\omega_{Lj}^2 = (\omega_{Pj}')^2 + (\omega_{Pj}'')^2 \qquad (5b)$$

$$\Gamma_{Tj} = -2\omega_{Zj}'' \qquad (5c)$$

$$\Gamma_{Lj} = -2\omega_{Pj}'' \qquad (5d)$$

Equation (4) then reduces to

$$\eta(\omega) = \prod_{j=1}^{N} \eta_\infty \frac{(\omega_{Tj}^2 - \omega^2 - i\Gamma_{Tj}\omega)}{(\omega_{Lj}^2 - \omega^2 - i\Gamma_{Lj}\omega)} \qquad (6)$$

The fundamental goal in an experimental analysis of $\epsilon(\omega)$ or $\eta(\omega)$ is to determine the location of the frequencies ω_{Tj} and ω_{Lj} and to determine the magnitude of the damping constants Γ_{Tj} and Γ_{Lj}. We consider here the case for $N = 2$ in Eq. (6) (This in fact provides a close approximation for the $\eta(\omega)$ response functions for most of the salts considered later). In this case, $\eta''(\omega)$, the imaginary part of $\eta(\omega)$, is given by

$$\eta''(\omega) = \frac{\eta_\infty}{\omega_L^4} \left[\frac{(\Gamma_L - \Gamma_T)\omega^3 + (\Gamma_T\omega_L^2 - \Gamma_L\omega_T^2)\omega}{\left(1 - \frac{\omega^2}{\omega_L^2}\right)^2 + \frac{\gamma^2\omega^2}{\omega_L^4}} \right] \qquad (7)$$

It is well-known that a maximum in the $\omega\epsilon''$ or $\frac{\epsilon''}{\omega}$ and $|\omega\eta''|$ or $|\frac{\eta''}{\omega}|$ for a classical oscillator dielectric response function (i.e., where $\Gamma_L = \Gamma_T$) will, respectively, exactly locate ω_T and ω_L. For real crystals, however, the classical oscillator model does not hold (since, for instance, $\Gamma_L \neq \Gamma_T$) and so we have

$$\left[\frac{\partial\omega\eta''}{\partial\omega} \right]_{\omega=\omega_L} = - \frac{2\eta_\infty\omega_L(\Gamma_L - \Gamma_T)}{\Gamma_L^2} \neq 0 \qquad (8)$$

$$\left[\frac{\partial \eta''/\omega}{\partial \omega}\right]_{\omega=\omega_L} = \frac{2\eta_\infty \omega_L}{\Gamma_L^2}\left(\frac{\Gamma_T \omega_L^2}{\omega_L^4} - \frac{\Gamma_L \omega_T^2}{\omega_L^4}\right) \neq 0 . \tag{9}$$

If a plane electromagnetic wave is to propagate through the system then we must have $\epsilon''(\omega) \geq 0$ and $\eta''(\omega) \leq 0$, which from Eq. (7) leads to the conclusion that

$$\Gamma_L - \Gamma_T \geq 0 \quad \text{and} \quad \Gamma_T \omega_L^2 - \Gamma_L \omega_T^2 \geq 0 . \tag{10}$$

Equations (8), (9), and (10) therefore reveal that the turning point in $\left[\frac{\partial \omega \eta''}{\partial \omega}\right]$ occurs at a frequency below ω_L and that the turning point in $\left[\frac{\partial \eta''/\omega}{\partial \omega}\right]$ occurs at a frequency above ω_L.[10] For the compounds investigated here the turning points in these two functions occur within 1 cm^{-1} of each other and so either of the functions may be used to conveniently locate ω_L. Exactly similar arguments can be used to define a frequency interval in which ω_T must exist from $\omega \epsilon''$ and ϵ''/ω functions.[10]

For systems where $\left(\frac{\Gamma_L}{\omega_L}\right)^2 \ll 1$, as is the case for nearly all the salts considered here, the width at half height of the functions $\omega \eta''$ and η''/ω are given, respectively, by $\Delta\omega_1$ and $\Delta\omega_2$ as

$$\Delta\omega_1 \approx \Gamma_L\left[1 - \frac{\Gamma_L}{2\omega_L}z_1 + \frac{1}{8}\frac{\Gamma_L^2}{\omega_L^2}z_1^2 \ldots\right] \tag{11a}$$

where

$$z_1 = \frac{1 + \dfrac{\omega_T^2}{\omega_L^2} - \dfrac{2\Gamma_T}{\Gamma_L}}{1 - \dfrac{\omega_T^2}{\omega_L^2}} .$$

and

$$\Delta\omega_2 \approx \Gamma_L\left[1 - \frac{\Gamma_L}{2\omega_L}Z_2 + \frac{\Gamma_L^2}{16\omega_L^2}Z_2^2 \dots \right]$$ (11b)

where

$$Z_2 = \frac{3 - \frac{\omega_T^2}{\omega_L^2} - \frac{2\Gamma_T}{\Gamma_L}}{1 - \frac{\omega_T^2}{\omega_L^2}} .$$

If $\Gamma_T = \Gamma_L$, as for the classical oscillator, then equations (11) reduce to the classical oscillator results (i.e., $\Gamma_L = \Gamma_T$):

$$\Delta\omega_1 \approx \Gamma_L\left(1 + \frac{\Gamma_L}{\omega_L}\right)$$

and

$$\Delta\omega_2 \approx \Gamma_L\left(1 - \frac{\Gamma_L}{\omega_L}\right) .$$

In a similar way the width at half height of the functions $\omega\epsilon''$ and ϵ''/ω are given, respectively, by $\Delta\omega_3$ and $\Delta\omega_4$ as:

$$\Delta\omega_3 \approx \Gamma_T\left(1 - \frac{\Gamma_T}{2\omega_T}Z_1 + \frac{1}{8}\frac{\Gamma_T^2}{\omega_T^2}Z_1^2 \dots\right)$$ (12a)

$$\Delta\omega_4 \approx \Gamma_T\left(1 - \frac{\Gamma_T}{2\omega_T}Z_2 + \frac{1}{16}\frac{\Gamma_T^2}{\omega_T^2}Z_2^2 \dots\right) .$$ (12b)

We find that $Z_1 \approx 1$ and $Z_2 \approx 2$ for the salts investigated here, so that only the first two terms in these expansions need be considered to obtain a good estimate of the values Γ_L and Γ_T. By separately determining ϵ'' and η'' as a

function of frequency, therefore, an iterative procedure involving, say, either Eqs. (11) or Eqs. (12) can be used to determine Γ_L and Γ_T. In the present work such an iterative procedure in many cases provided adjustments of less than 5% to the values of Γ_L determined as the value of $\Delta\omega_1$ or $\Delta\omega_2$. Since for the main part such adjustments were less than the experimental error, the values of Γ_L were taken directly as the half height widths $\Delta\omega_1$ or $\Delta\omega_2$.

The frequency dependence of η'' or ϵ'' is readily obtained from a Kramers-Kronig analysis of reflectance measurements using the Fresnel formulae appropriate for a crystal aligned with the desired axis precisely parallel to the incident electric field and perpendicular to the plane of incidence. However, as Berreman[5] first demonstrated, the longitudinal optic modes can be more directly studied from thin film measurements. The π polarized reflectance component, R_π, of a thin film on a conducting substrate is given to a good approximation by

$$1 - R_\pi = - A\omega\eta''$$

with

$$A = \frac{4d}{c} \frac{\sin^2\theta}{\cos\theta}$$

where θ is the angle of incidence, c is the velocity of light and d is the film thickness. Since A will be constant in any one experiment, it is clear from the previous discussion that ω_L will be located by the frequency position of the maximum of $\frac{1 - R_\pi}{\omega^2}$ and that Γ_L will be determined to a good approximation by measuring the width of the curve of $\frac{1 - R_\pi}{\omega^2}$ at $R_\pi = \frac{1 + R_\pi^L}{2}$ where R_π^L is the magnitude of R_π at $\omega = \omega_L$.

3. EXPERIMENT

The infrared spectroscopic measurements to determine the dispersion of η'' in the region of ω_L were recorded partly on an f2 single pass grating instrument of the Ebert type and partly with an R.I.I.C. (London) 520 Fourier spectrophotometer used in conjunction with a liquid helium cooled Ga doped germanium bolometer.

The frequency dependence of η'' was determined for most salts from a measurement of R_π (angle of incidence $\approx 80°$) for thin films evaporated on aluminized mirrors. Many of the compounds were hygroscopic to some extent. An evaporation gun was therefore incorporated into the low temperature cryostat and the thin films of these more hygroscopic compounds were prepared in situ without exposing them to the atmosphere. For a few compounds, $\eta''(\omega)$ was also determined from Kramers-Kronig analyses of reflectance data taken at near normal incidence (angle of incidence $\approx 7\frac{1}{2}°$) from single crystal samples.

High pressure spectroscopic studies of ω_L were made using the far infrared pressure bomb shown in Fig. 1. The pressure bomb is capable of operating up to 10 kilobars using either dry nitrogen or argon gas as the compression medium. In the present experiments the pressure was delivered to the bomb by a Harts compressor. The radiation ports in the bomb were 1 cm in diameter and consisted of two 5 cm diameter crystal quartz blanks, lapped optically flat and parallel to better than 300 Å with the martensitic steel window mounts E. An elliptical specimen holder D containing a sample port and a blank reference port was manually operated externally to the bomb by rotating the control changer C, thus permitting both sample and reference spectra to be recorded without changing the internal environmental condition of the bomb. In studying the pressure dependence of ω_L large incident angle transmission measurements

on thin films on lossless substrates were used.[5] The use of the radiation

guide and cone in the support window plugs B ensured that the radiation, through

repeated reflection, would strike the samples mounted in the plane of D (per-

pendicular to the figure plane) at large angles of incidence.

4. RESULTS

Figure 2 shows the measured reflectance at near normal incidence from bulk samples of KBr, RbI, CsI and TlBr at different temperatures and compares the frequency dependence of $\frac{\eta''}{\omega}$ determined from Kramers-Kronig analyses of this reflectance data with the frequency dependence of $\frac{(1 - R_\pi)}{\omega^2}$ determined from the small grazing angle reflectance of thin films. Also shown for completeness are the functions $\omega\varepsilon''$, determined from bulk crystal reflectance data, and the function $\left(\frac{1}{T} - 1\right)$ determined from the transmittance, T, of thin films on lossless substrates (polystyrene or mica) for near normal incident radiation. The figures reveal that the location of ω_L, determined from the frequency position of the turning point in $\frac{\eta''}{\omega}$, are in close agreement for the two methods of determination. In addition, the line shape, as defined by the profiles of $\frac{\eta''}{\omega}$ are in reasonable agreement for both types of measurement.

Table 1 summarizes values of ω_L for eighteen salts in the temperature range $5°-400°K$ determined from both types of experimental measurement. The measuring accuracy is better than ±0.5 cm^{-1}. Where there is overlap between the two measuring techniques it can be seen that there is overall agreement between the frequencies to better than 1%. The spectra for several of the compounds showed strong subsidiary bands in the close proximity of the fundamental longitudinal optic modes, as illustrated in Fig. 3 for KBr, and the frequencies of these subsidiary bands are indicated in the table by an asterisk. These side bands are thought to be associated with two phonon decay and scattering processes.

Table 2 lists the observed values of $\frac{\Gamma_L}{\omega_L}$ determined from the thin film and single crystal measurements. For those salts where the line profile close to ω_L contains a distinct double peak it is clear that the simplified analysis of section 2 to obtain Γ_L does not apply. No values of $\frac{\Gamma_L}{\omega_L}$ have therefore been

included in Table 2 for such cases. Data are not included for KF and RbF at

other than 5°K partly because the widths at half height were too large at

higher temperatures for the approximations contained in section 2 to hold and

partly because of the comparatively large error involved in measuring these

widths. It is not clear whether these large values of $\frac{\Gamma_L}{\omega_L}$ reflect a genuine

short lifetime for these LO phonons or whether it is to some extent an artifact

due to the less pure starting material used in the preparation of these films.

As Table 2 shows, the lifetimes of the $k \approx 0$ LO phonons in the alkali halides

are significantly shorter than those of the $k \approx 0$ TO phonons.

Figure 3 shows the pressure dependence of the $k \approx 0$ LO frequencies

of RbI and CsI for pressures up to 5 kilobars at 290°K. Even though the pres-

sure induced shifts were small, because of the point by point measuring

technique used and the lack of any observable hysteresis during the pressur-

izing cycle, the measurements of $\left[\frac{\partial \omega}{\partial P}\right]_T$ are thought to have an accuracy within

$\pm 15\%$.

5. DISCUSSION

5.1 The Lyddane-Sachs-Teller Relation

On the basis of a simple microscopic model of the dielectric
properties of cubic diatomic ionic solids, Lyddane, Sachs and Teller[11]
obtained the relation

$$\omega_L^2 = \omega_T^2 \frac{\epsilon_o}{\epsilon_\infty} .$$

The assumptions based in their derivation of this relation were that the equa-
tion of motion and polarization of the system varies linearly as the amplitude
of the applied field and that the effective polarizing field at a lattice site
depends on the macroscopic and Lorentz internal field. The relation is some-
what more general than was first implied, however, and it is readily shown that
the relation follows from causal behavior provided the ϵ'' curve exhibits a
delta function at ω_T. Cochran and Cowley[12] have shown that the relation holds
in any crystallographic direction for crystals of any symmetry within the
adiabatic, electrostatic and harmonic approximation. The comparatively few
measurements of ω_L for any solids have prevented any rigorous overall assess-
ment of the LST relation. Neutron scattering measurements have determined ω_L
for KBr,[13] NaI,[13] KI,[14] TlBr[15] and NaCl[16] at 90°K, and some verifica-
tions have been made for piezoelectric crystals where the optic modes are
simultaneously infrared and Raman active.[17] Using the recently reported
values of ω_T, ϵ_o and ϵ_∞ for the salts considered here,[2] values of ω_L have been
calculated for temperatures of 5° and 290°K and these are listed in Table 1.
The results indicate that the LST relation holds to better than 3% at 5°K and is
in reasonably good agreement even at 290°K although discrepancies of as much as
10% were noted in some cases. The degree of agreement at low temperatures is
encouraging and provides some support for the use of the harmonic approximation
in lattice dynamical calculations for these salts at temperatures close to
0°K. (18,19)

5.2 The One-Phonon Longitudinal Optic Gruneisen Parameters

The temperature dependence of each phonon frequency in the Brillouin zone stems from the anharmonic terms in the lattice potential energy in two separate ways. Firstly, due to the thermal expansion of the crystal, the inter-ionic force constants are temperature dependent, thus creating a quasi-harmonic shift of each phonon frequency as the temperature (i.e., volume) changes. Secondly, lattice anharmonicity allows interactions between phonons of different modes and these interactions will change the phonon energies and give them a finite lifetime. Since the probability of such interactions occurring depends on the phonon occupation number, it is clear that both the phonon frequency and lifetime will have a temperature dependence which will take place even under constant volume.

We consider first the variations of ω_L with volume. Within the limits of a quasiharmonic oscillator model, the volume dependence of the $k \approx 0$ longitudinal optic mode frequency is described by

$$\gamma_L = - \left[\frac{\partial \ell n \omega_L}{\partial \ell n V} \right]_T \tag{13}$$

where γ_L is the characteristic Gruneisen parameter for the LO mode. The Gruneisen parameter can be conveniently determined experimentally from the relation

$$\gamma_L = \frac{1}{\beta \omega_L} \left[\frac{\partial \omega_L}{\partial P} \right]_T \tag{14}$$

providing the compressibility, β, and the pressure coefficient under constant temperature of ω_L, $\frac{1}{\omega_L} \left[\frac{\partial \omega_L}{\partial P} \right]_T$, are known. Using the measured pressure dependence of ω_L reported here, the Gruneisen parameters for the $k \approx 0$ LO modes of RbI, CsBr and CsI have been calculated and are listed in Table 3.

An estimate of the Gruneisen constant γ_L for the remaining salts can be calculated from Szigeti's treatment of the static dielectric constant of cubic ionic crystals.[20] Szigeti obtains the following form for the static dielectric constant, ϵ_o

$$\epsilon_o = \epsilon_\infty + \left(\frac{\epsilon_\infty + 2}{3}\right) \frac{24\pi e^{*2}}{\mu v \omega_T^2} + G \tag{15}$$

where ϵ_∞ is the high frequency dielectric constant, e^* is the Szigeti effective charge,[21] and μ and v are the reduced mass and cell volume, respectively, for a cell unit. G is the pure anharmonic contribution to ϵ_o and in Szigeti's treatment is assumed to be volume independent. From the previous section it was clear that even at $290^\circ K$ the LST relation held to a good approximation, so that Eq. (15) can be reduced to

$$\epsilon_o \approx \epsilon_\infty + \left(\frac{\epsilon_\infty + 2}{3}\right)^2 \frac{4\pi e^{*2}}{\mu v \omega_L^2} \cdot \frac{\epsilon_o}{\epsilon_\infty} + G. \tag{16}$$

Differentiating Eq. (16) leads to

$$\gamma_L = -\left[\frac{\partial \ln \omega_L}{\partial \ln V}\right]_T = \frac{1}{2}\left[\frac{\partial \ln(\epsilon_o - \epsilon_\infty)}{\partial \ln V}\right]_T + \frac{1}{2}\left[\frac{\partial \ln \epsilon_\infty}{\partial \ln V}\right]_T$$

$$- \left[\frac{\partial \ln(\epsilon_\infty + 2)}{\partial \ln V}\right]_T - \left[\frac{\partial \ln e^*}{\partial \ln V}\right]_T - \frac{1}{2}\left[\frac{\partial \ln \epsilon_o}{\partial \ln V}\right]_T + \frac{1}{2} . \tag{17}$$

The main difficulty in assessing γ_L from Eq. (17) is the calculation of the volume dependence of e^*. Born and Huang[22] have shown where distortion dipoles directed along anion-cation bonds are responsible for e^*, that

$$e^* - e = \frac{N}{3}\left[m'(r_o) + \frac{2m(r_o)}{r_o}\right] \tag{18}$$

where N is the lattice coordination number, $m(r_o)$ is the distortion dipole

between nearest neighbors at their equilibrium separation of r_o, and $m'(r_o)$ is the rate of change of $m(r_o)$ with lattice spacing. Mitskevich,[23] and Lowndes and Martin[2] have pointed out that the distortion dipole moment in those alkali halides crystallizing in the NaCl structure contains a contribution arising from short-range Coulomb interactions between the hexadecapole moments of an ion and the monopole moments of its immediate neighbors, as well as the more established contribution from the short-range repulsive forces. It is found that[2,23] the total value of $m(r)$ is closely described by the form

$$m(r) = Ae^{-r/\rho}$$

where A is a constant, and r and ρ are the nearest neighbor distance and the hardness parameter, respectively, as given by Born and Huang.[22] Assuming this to be generally true, Eq. (18) leads to

$$\frac{d\ln e^*}{d\ln V} = \frac{\left[\frac{e}{e^*} - 1\right]\left[\frac{r_o}{\rho^2} - \frac{2}{\rho} - \frac{2}{r_o}\right]}{3\left[\frac{1}{\rho} - \frac{2}{r_o}\right]} . \tag{19}$$

Using the available data for $\frac{e^*}{e}$[2] and ρ and r_o[22] together with available data for the volume dependence of ϵ_o[24] and ϵ_∞[25,26] allows an estimate of γ_L to be determined from Eq. (17). The values of γ_L so calculated are listed in Table 4 and it can be seen that for those salts where γ_L was determined directly from experimental measurements there is good agreement between the calculated and experimental values.

5.3 The Self-Energy of the Longitudinal Optic Modes

We consider now the self-energy contribution to the overall temperature dependence of the longitudinal optic modes. From the previous section we may write the longitudinal optic frequency, $\omega_L(T)$, in the form

$$\omega_L(T) = \omega_L(0) - \Delta\omega_L^E(T) - \Delta\omega_L^A(T) \tag{20}$$

where $\omega_L(0)$ is the frequency at $0^\circ K$ and $\Delta\omega_L^E(T)$ is the quasi-harmonic shift due to thermal expansion and $\Delta\omega_L^A(T)$ is the self-energy shift. The quasi-harmonic shift is defined as

$$\Delta\omega_L^E(T) = \omega_L(0) - \omega_L^E(T) \tag{21}$$

where $\omega_L^E(T)$ is the characteristic frequency at temperature T that the solid would have if thermal expansion processes only were responsible for the temperature dependence of ω_L. The quantity $\omega_L^E(T)$ can be calculated from

$$\ln\omega_L^E(T) = \ln\omega_L(0) - \gamma_L \int_0^T \alpha dT \tag{22}$$

where α is the volume coefficient of expansion. The self-energy shift is defined by

$$\Delta\omega_L^A(T) = \omega_L^E(T) - \omega_L(T) \tag{23}$$

where $\omega_L^A(T)$ is the characteristic frequency at temperature T that would be recorded for a solid held under constant volume between $T = 0$ and a temperature T.

Values of $\Delta\omega_L^E$ and $\Delta\omega_L^A$ determined from Eqs. (21) and (23) are summarized in Table 3 for the temperatures 80°, 200° and $290^\circ K$. Values of α used in the

calculation of $\Delta\omega_L^E$ were taken from the literature.[27-31] A comparison of the magnitudes of $\Delta\omega_L^A$ (290) reveals that as we move from the heavier Rb halides to the lighter Li halides the magnitude of the self-energy shift decreases significantly. In the case of the Rb and K halides, for example, the self-energy shift strongly dominates the shift due to thermal expansion, whilst the reverse is true for the Na and Li halides. In the Cs halides the $\Delta\omega_L^E$ (290) also dominates the $\Delta\omega_L^A$ (290) but now these quantities are opposed in sign unlike the results for the other alkali halides. The calculations show a reversal in the sign of the $\Delta\omega_L^A$ for the Cs halides at temperatures below 200°K. Similarly the calculations show the $\Delta\omega_L^A$ for the Na salts to be decreasing with increasing temperature so that the possibility exists that there could be a change in sign for these salts for the $\Delta\omega_L^A$ at temperatures higher than 290°K. However, because of the approximations made in the calculations of γ_L and because of the experimental uncertainties in the various quantities used in these calculations, the small magnitudes of $\Delta\omega_L^A$ (290) determined here for LiF, NaF, NaCl and CsCl do not decisively decide the sign of $\Delta\omega_L^A$ (290) for these salts; for the same reasons the calculations do not conclusively indicate that a reversal of sign for $\Delta\omega_L^A$ does take place for the Cs or Na salts.

A number of authors have deduced expressions for $\Delta\omega_L^A$ by perturbation theory (see review by Cowley[32]). Maradudin and Fein[33] have calculated the effect of cubic anharmonicity to second order and of quartic anharmonicity to first order in perturbation theory and they obtain an expression for $\Delta\omega_L^A$ of

$$\Delta\omega_L^A = +\frac{18}{\hbar^2}\sum_{q_1 q_2 j_1 j_2}\left|V\begin{pmatrix}0 & q_1 & q_2\\ L & j_1 & j_2\end{pmatrix}\right|^2\left\{\frac{n_1+n_2+1}{\omega_1+\omega_2+\omega_L}+\frac{n_1+n_2+1}{\omega_1+\omega_2-\omega_L}\right.$$

$$\left.+\frac{n_2-n_1}{\omega_1-\omega_2+\omega_L}+\frac{n_2-n_1}{\omega_1-\omega_2-\omega_L}\right\}-\frac{12}{\hbar}\sum_{q_1 j_1}V\begin{pmatrix}0 & 0 & q_1 & -q_1\\ L & L & j_1 & j_1\end{pmatrix}\{2n_1+1\}$$

(24)

where $n_1 = n(\underset{\sim}{q_1} j_1)$ is the thermal expectation value for the occupation number

of the phonon mode and $\omega_1 = \omega(\underset{\sim}{q_1} j_1)$ is its frequency. The V coefficients

derive from the lattice potential energy of deformation at constant volume,

expanded in terms of the normal phonon coordinates. Equation (24) shows $\Delta\omega_L^A$

to be the sum of a positive term related to the cubic term in V and a term

which derives from the quartic term in V which may be negative. The negative

values found for $\Delta\omega_L^A$ at $290^{\circ}K$ for the Cs halides would seem to indicate that

the quartic contribution is indeed negative and that in these cases this

dominates the contribution from the cubic term. The small values of $\Delta\omega_L^A$ (290)

determined for the Li and Na halides suggest that there is a near cancellation

of the cubic and quartic terms in V at $290^{\circ}K$ whilst the relatively large

positive values of $\Delta\omega_L^A$ (290) determined for the K and Rb salts clearly

indicate that the cubic terms in V provide the dominant contribution to $\Delta\omega_L^A$

for these salts. The reason for the dominance in $\Delta\omega_L^A$ of the contributions

from quartic terms in V for compounds which have the CsCl structure is not

clear. Bosman and Havinga have suggested that the cubic terms could be of

reduced significance in a CsCl structure because the higher coordination

number reduces the effect of fluctuations among the pairs of bonds formed by

an ion with its neighbors. [34]

It is worth-noting that $\Delta\omega_L^A(0)$ is not zero because anharmonic

contributions exist in the presence of zero point fluctuations. However,

extrapolations of the data in Tables 1 and 4 suggest that the $\Delta\omega_L^A(0)$ are not

much larger than 1% of $\omega_L(0)$. This near zero value of $\Delta\omega_L^A(0)$ may in fact be

the reason why the observed values of $\omega_L(5)$ are nearly always 1-2% lower than

the values calculated from the LST relation.

The general formula for the inverse lifetime given by Maradudin and

Fein[33] can be reduced to describe the one phonon main transition in the

vicinity of ω_L as a damped Lorentzian resonance with a damping parameter Γ_L given by

$$\Gamma_L \doteq \frac{18\pi}{\hbar^2} \sum_{q_2 q_1 j_1 j_2} \left| V \begin{pmatrix} 0 & q_1 & q_2 \\ L & j_1 & j_2 \end{pmatrix} \right|^2 \left[(n_1 + n_2 + 1)\delta^S + (n_2 - n_1)\delta^D \right] \quad (25)$$

where δ^S and δ^D are Dirac δ functions which are zero except for pairs of modes

for which ω_L is near $(\omega_1 + \omega_2)$ and $(\omega_2 - \omega_1)$, respectively. Equation (25)

reveals that $\Gamma_L \neq 0$ even at $T = 0^\circ K$. Extrapolations of the measured temper-

ature dependence of Γ_L down to $5^\circ K$ confirm this result. Equation (25) shows

that the decay of the phonon at ω_L is proportional to the two phonon density

of states at ω_L. The strong attenuation at ω_L for many salts, especially for

the double peak profiles found in NaCl, KCl, KBr, KI, and RbCl are therefore

probably due to the presence of peaks in the two phonon density of states at

or near ω_L. The existence of a double peak feature near ω_L for KCl and RbCl

at $5^\circ K$ implies that these are due primarily to two phonon summation processes.

A test of the observed temperature dependence of $\Delta\omega_L^A$ and Γ_L against

the theoretical expressions in Eqs. (24) and (25) would require the evaluation

of extensive summations over one and two phonon densities of states. Some

simplification to the problem is achieved if we restrict our interest to tem-

peratures higher (but not too high) than the effective Debye temperature for

the salts, since at these temperatures the leading terms in expansions of the

n_i give a linear temperature dependence of both $\Delta\omega_L^A$ and Γ_L. More detailed

measurements of the temperature dependence of ω_L and Γ under constant pressure

and constant volume are currently being made to temperatures well above the

characteristic Debye temperatures of these salts in order to test these pre-

dictions. However, it is of interest to compare the values of $\Delta\omega_L^E$ and $\Delta\omega_L^A$

presented here with the shell model calculations made by Cowley[35] for KBr.

Table 5 shows that whilst the overall temperature dependence of ω_L for KBr is

in good agreement, the $\Delta\omega_L^E$ and $\Delta\omega_L^A$ obtained from the present work vary more

slowly and more quickly with temperature, respectively, than indicated by

Cowley's calculations.

SUMMARY

The measurement of the temperature and pressure dependence of the $k \approx 0$ LO modes of simple cubic ionic solids has allowed a first determination of the variation of ω_L at constant volume and of the magnitude of the self-energy contribution to these modes. The measurements reveal that the self-energies of these modes at $290^{\circ}K$ can either enhance or oppose the temperature dependence of the modes arising from thermal expansion, depending on whether three phonon processes due to cubic anharmonicity or four phonon processes due to quartic anharmonicity give the overriding contribution to the self-energies. At $0^{\circ}K$ only small residual self-energy contributions appear to remain which amount to no more than 1% of the total LO phonon energies.

REFERENCES

1. G. O. Jones, D. H. Martin, P. A. Mawer and C. H. Perry, Proc. Roy. Soc., A261, 10 (1961).

2. R. P. Lowndes and D. H. Martin, Proc. Roy. Soc., A308, 473 (1969).

3. S. S. Mitra, C. Postmus and J. R. Ferraro, Phys. Rev. Letters 18, 455 (1967).

4. C. Postmus, J. R. Ferraro and S. S. Mitra, Phys. Rev. 174, 983 (1968).

5. D. W. Berreman, Phys. Rev. 130, 2193 (1963).

6. R. P. Lowndes, J. F. Parrish and C. H. Perry, Phys. Rev. 182, 913 (1969).

7. A. S. Barker in Ferroelectricity, edited by E. F. Weller (Elsevier Publishing Company, Amsterdam 1967).

8. A. S. Davidov in Quantum Mechanics, translated and edited by D. ter Haar (Addison-Wesley Publishing Company, 1965), Section 112.

9. D. W. Berreman and F. C. Unterwald, Phys. Rev. 174, 791 (1968).

10. J. F. Parrish, M.I.T. Quarterly Progress Report 90, 37 (1968).

11. R. H. Lyddane, R. G. Sachs and E. Teller, Phys. Rev. 59, 673 (1941).

12. W. Cochran and R. A. Cowley, J. Phys. Chem. Solids 23, 447 (1962).

13. A. D. B. Woods, B. N. Brockhouse and R. A. Cowley, Phys. Rev. 131, 1025 (1963).

14. G. Dolling, R. A. Cowley, C. Schittenhelm and I. M. Thorson, Phys. Rev. 147, 577 (1966).

15. E. R. Cowley and A. Okazaki, Proc. Roy. Soc. 300A, 45 (1967).

16. G. Raunio, L. Almqvist and R. Stedman, Phys. Rev. 178, 1496 (1969).

17. R. Loudon, Advances in Physics 14, 423 (1964).

18. A. D. B. Woods, W. Cochran and B. N. Brockhouse, Phys. Rev. 119, 980 (1960).

19. A. M. Karo and J. R. Hardy, Phys. Rev. 129, 2024 (1963).

20. B. Szigeti, Proc. Roy. Soc. A261, 274 (1961).

21. B. Szigeti, Trans. Faraday Soc. 45, 155 (1949).

22. M. Born and K. Huang, Dynamical Theory of Crystal Lattices (Oxford University Press, New York 1954), pp.

23. V. V. Mitskevich, Sov. Phys.-Sol. State 5, 2568 (1964).

24. R. P. Lowndes and D. H. Martin, Proc. Roy Soc. (in press).

25. E. Burstein and P. L. Smith, Phys. Rev. 74, 229 (1948).

26. H. Leibssle, Z. Krist. 114, 457 (1960).

27. F. A. Henglein, Z. Phys. Chem. A115, 91 (1925).

28. B. Yates and C. H. Panter, Proc. Phys. Soc. 80, 373 (1962).

29. G. K. White, Proc. Roy. Soc. A286, 204 (1965).

30. B. W. James and B. Yates, Phil. Mag. 7, 663 (1965).

31. A. C. Bailey and B. Yates, Phil. Mag. 18, 1241 (1968).

32. R. A. Cowley, Rep. Prog. Phys. 31, Part 1, 123 (1968).

33. A. A. Maradudin and A. E. Fein, Phys. Rev. 128, 2589 (1962).

34. E. E. Havinga and A. J. Bosman, Phys. Rev. 140, 292 (1965).

35. R. A. Cowley, Advances in Physics, 12, 421 (1963).

TABLE CAPTIONS

Table 1   Values of ω_L, in cm^{-1}, as determined from Kramers-Kronig (KK)

analyses of reflectance data, from small grazing angle thin

film reflectance data (film) and from the Lyddane-Sachs-

Teller (LST) relation. The neutron measurements are taken

from references 13-15. An asterisk indicates the frequency

location of side bands in the close vicinity of ω_L. The

experimental accuracy is ± 0.5 cm^{-1}.

Table 2   Values of $\dfrac{\Gamma_L}{\omega_L}$ determined from KK analyses and from thin film

measurements. The Γ_T are taken from reference 10.

Table 3   Values of $\dfrac{1}{\omega}\left[\dfrac{\partial \omega}{\partial P}\right]_T$ and γ_L for RbI, CsBr and CsI.

Table 4   Calculated values of γ_L, $\Delta\omega_L^E$ and $\Delta\omega_L^A$ for several salts.

All frequencies are in cm^{-1}. An asterisk indicates an

experimental value of γ_L.

Table 5   A comparison of values for $\Delta\omega_L^E$, $\Delta\omega_L^A$ and $\Delta\omega_L$ (in cm^{-1}) for

KBr obtained from the present work with the shell model

calculations of Cowley.

Table 1

	400°K Film	400°K KK	290°K Film	290°K KK	290°K LST	200°K Film	200°K KK	90°K Neutron	80°K Film	80°K KK	5°K Film	5°K KK	5°K LST
LiF			670	671	661	672	672		673	673	673	673	671
LiCl			425		421	429			433		435		435
NaF			421.5			424			426		426		431
NaCl			250*, 263		261	264		264	265		266		271
NaBr			202		208	206			210		212		216
NaI			164		180			172	172		174		181
KF			330		335						335		335
KCl			198, 220*	198.5; 218*	211	204, 222*	205, 223*		210, 224*	211.5, 228*	212, 226*	212, 228*	212
KBr	157, 17	150, 170*	157, 173*	157 ; 175*	165	161	161	167	165	164	166	166	170
KI			127, 145*	145	142	134	134.5	142	141	141	143	143.5	145
RbF			285		290						290		286
RbCl			167, 191*		175	173, 195*			180, 200*		182, 200*		181
RbBr			128		126	130			133		134		130
RbI	88	86	97.5	95	104	101	100		104	104	105.5	105.5	108
CsCl	158		160		162	161.5			162.5		163		168
CsBr	112		113		114	113.5			114		115		115
CsI	89.5	89.5	90.5	90.5	91	91	91		91	91.5	91.5	91.5	94
TlBr	114	115	115.5	116	117	116	116	112	117.5	116	118	117	118

Table 2

	5°K			80°K		200°K		290°K		
	KK	Film	$\frac{\Gamma_L}{\Gamma_T}$	KK	Film	KK	Film	KK	Film	$\frac{\Gamma_L}{\Gamma_T}$
LiF	0.040	0.045	4.2	0.060	0.060	0.075	0.080	0.090	0.100	3.9
LiCl		0.130	4.0		0.160		0.260		0.340	4.2
NaF		0.050	3.2		0.070		0.120		0.170	4.2
NaCl	0.045	0.050	4.9		0.070					
NaBr		0.070	4.4		0.110		0.170		0.220	5.3
NaI		0.090	4.2		0.120		0.180		0.230	4.0
KF		0.090	2.5							
KBr	0.035	0.050	9.0	0.055	0.070					
KI	0.050	0.055	4.2	0.057	0.080					
RbF		0.080	3.6							
RbCl		0.060	4.2		0.075		0.110		0.160	5.7
RbBr		0.070	6.8		0.105		0.140		0.170	7.3
RbI	0.060	0.075	6.5	0.085	0.100	0.105	0.125	0.125	0.150	5.2
CsCl		0.100	4.5		0.120		0.165		0.205	5.4
CsBr		0.055	4.3		0.065		0.080		0.100	2.8
CsI	0.115	0.065	5.6	0.125	0.090	0.140	0.120	0.170	0.160	5.5
TlBr	0.060	0.070	2.0	0.075	0.080	0.125	0.120	0.170	0.150	2.6

Table 3

	β 10^{-12} cm^{2}dyne^{-1}	ω_L cm^{-1}	$\frac{1}{\omega_L}\left[\frac{\partial\omega_L}{\partial P}\right]_T$ 10^{-12} cm^{2}dyne^{-1}	γ_L
RbI	9.66	97.5	7.3	0.76
CsBr	6.69	113.0	4.2	0.63
CsI	8.40	89.5	5.7	0.68

Table 4

	γ_L	$\omega_L(0)$	$\Delta\omega_L^E(80)$	$\Delta\omega_L^A(80)$	$\Delta\omega_L^E(200)$	$\Delta\omega_L^A(200)$	$\Delta\omega_L^E(290)$	$\Delta\omega_L^A(290)$
LiF	0.22	673	0	0	1.0	0	2.2	0.8
NaF	0.67	426	0.2	0.3	2.3	0.3	4.3	0.2
NaCl	0.47	271	0.1	0.9	1.6	0.4	2.9	0.1
KCl	0.58	212	0.3	1.7	1.6	6.4	2.7	11.3
KBr	0.60	166	0.3	0.7	1.5	3.5	2.5	6.5
KI	0.51	143	0.2	1.8	1.2	7.8	2.1	13.9
RbCl	0.63	182	0.1	1.9	1.3	7.7	2.5	12.5
RbBr	0.58	134	0.2	0.8	1.2	2.8	2.0	4.0
RbI	0.52	105.5	0.3	1.2	0.9	3.6	1.5	6.5
RbI	0.76*	105.5	0.3	1.2	1.3	3.2	2.2	5.8
CsCl	0.64	163	0.6	-0.1	1.9	-0.4	3.8	-0.8
CsBr	0.57	115	0.3	0.7	1.3	0.2	2.2	-0.2
CsBr	0.63*	115	0.4	0.6	1.6	-0.1	2.5	-0.5
CsI	0.50	91.5	0.3	0.2	1.0	-0.5	1.6	-0.6
CsI	0.68*	91.5	0.4	0.1	1.3	-0.8	2.1	-1.1

Table 5

|	80°K Present Work	90°K Cowley	200°K Present Work	Cowley	290°K Present Work	Cowley
$\Delta\omega_L^E$	0.3	3.4	1.5	6.5	2.5	9.2
$\Delta\omega_L^A$	1.7	-0.5	3.5	1.3	6.5	1.9
$\Delta\omega_L$	2.0	2.9	5.0	7.8	9.0	11.9

FIGURE CAPTIONS

Figure 1   The far infrared high pressure cell. A, cell body;

B, window plugs; C, specimen changer; D, specimen holder;

E, window mount; F, crystal quartz window; G, high
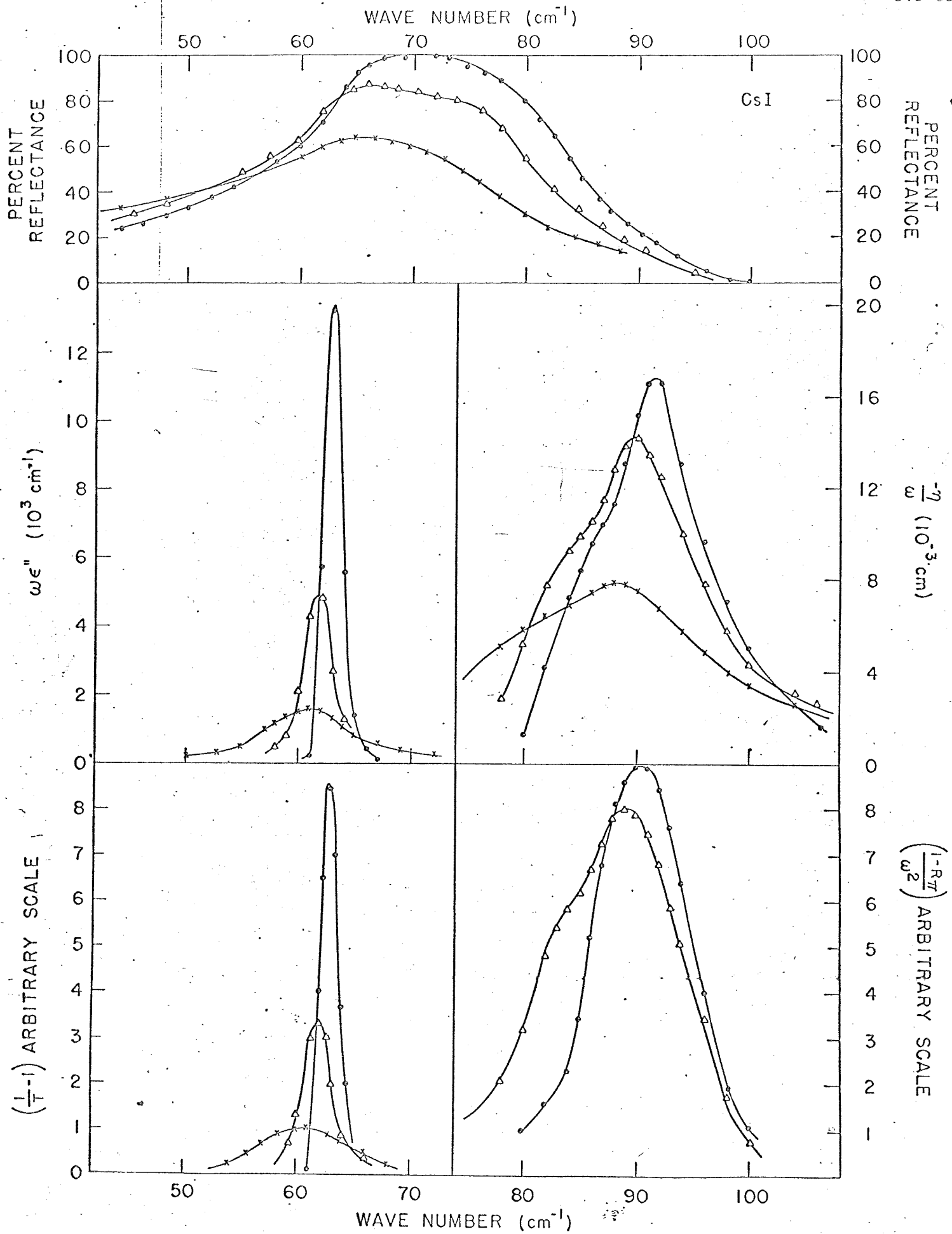
pressure transmission line inlet.

Figure 2   The temperature dependence of the reflectance and dielectric

functions $\omega\varepsilon''$ and $-\dfrac{\eta''}{\omega}$ for a) KBr, b) RbI, c) CsI, d) TlBr.

⊙——⊙ 5°K, ○——○ 80°K, △——△ 290°K, x——x 400°K.
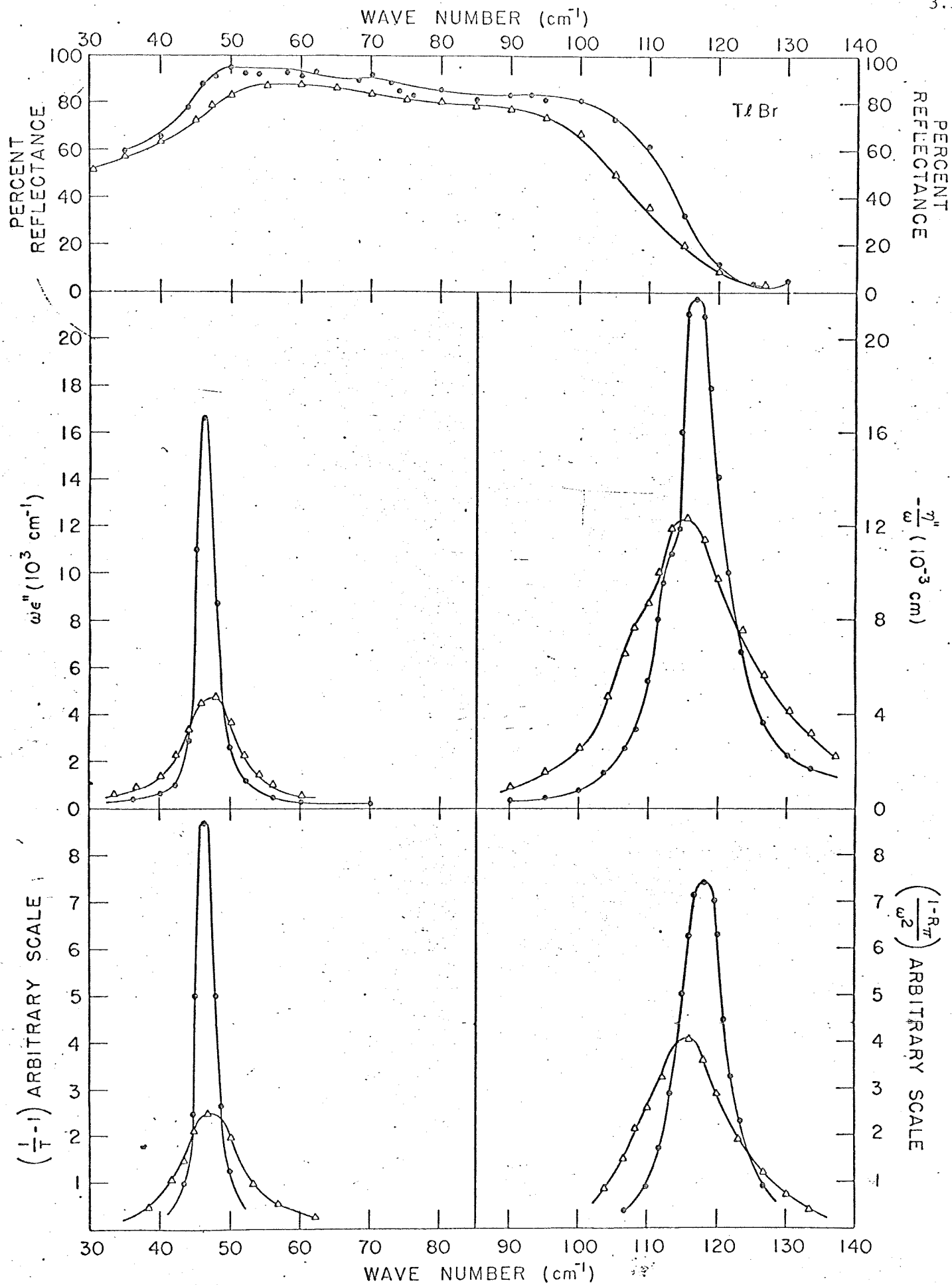
Figure 3   The measured pressure dependence of ω_L for RbI and CsI.
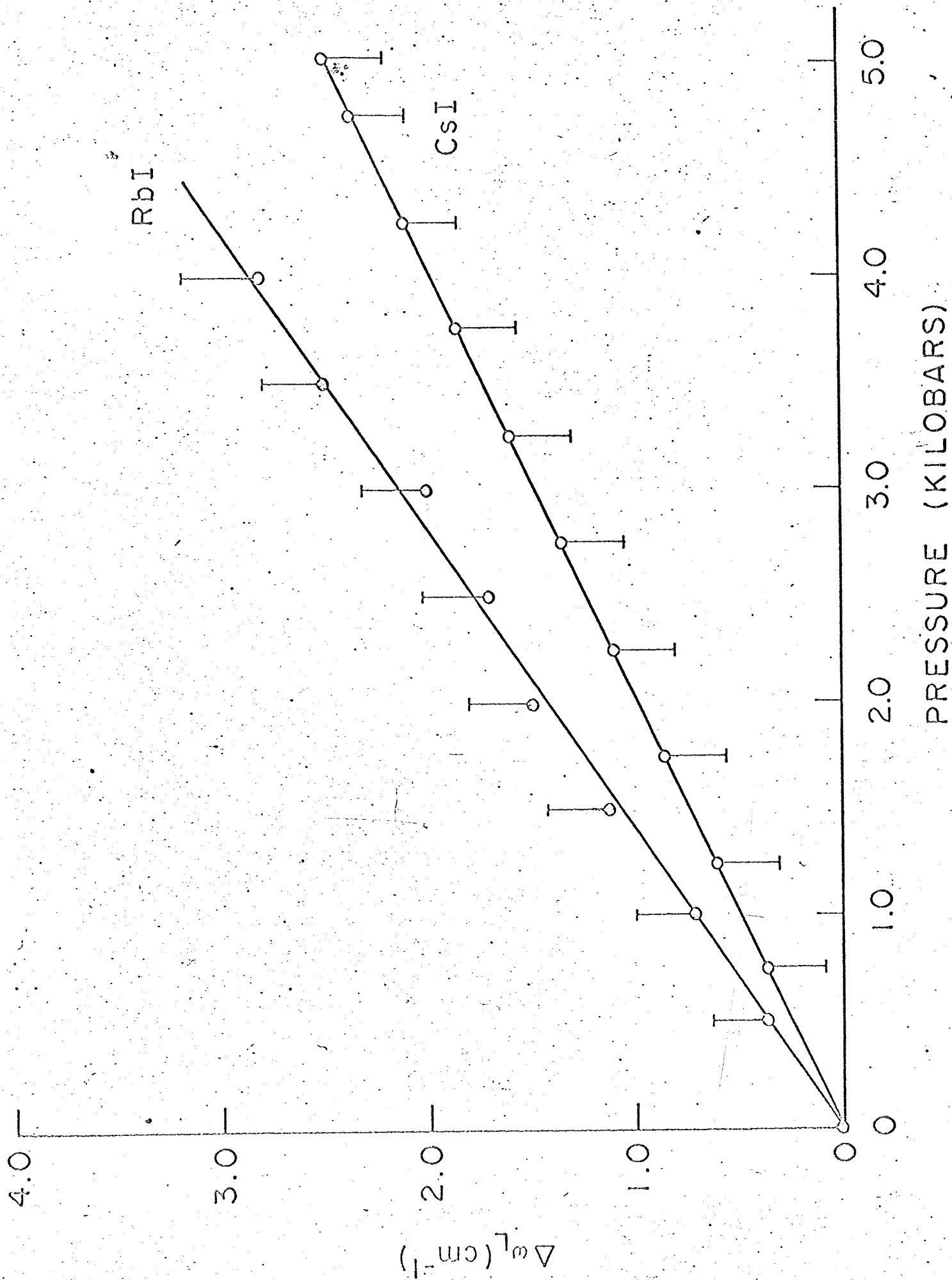
TℓBr
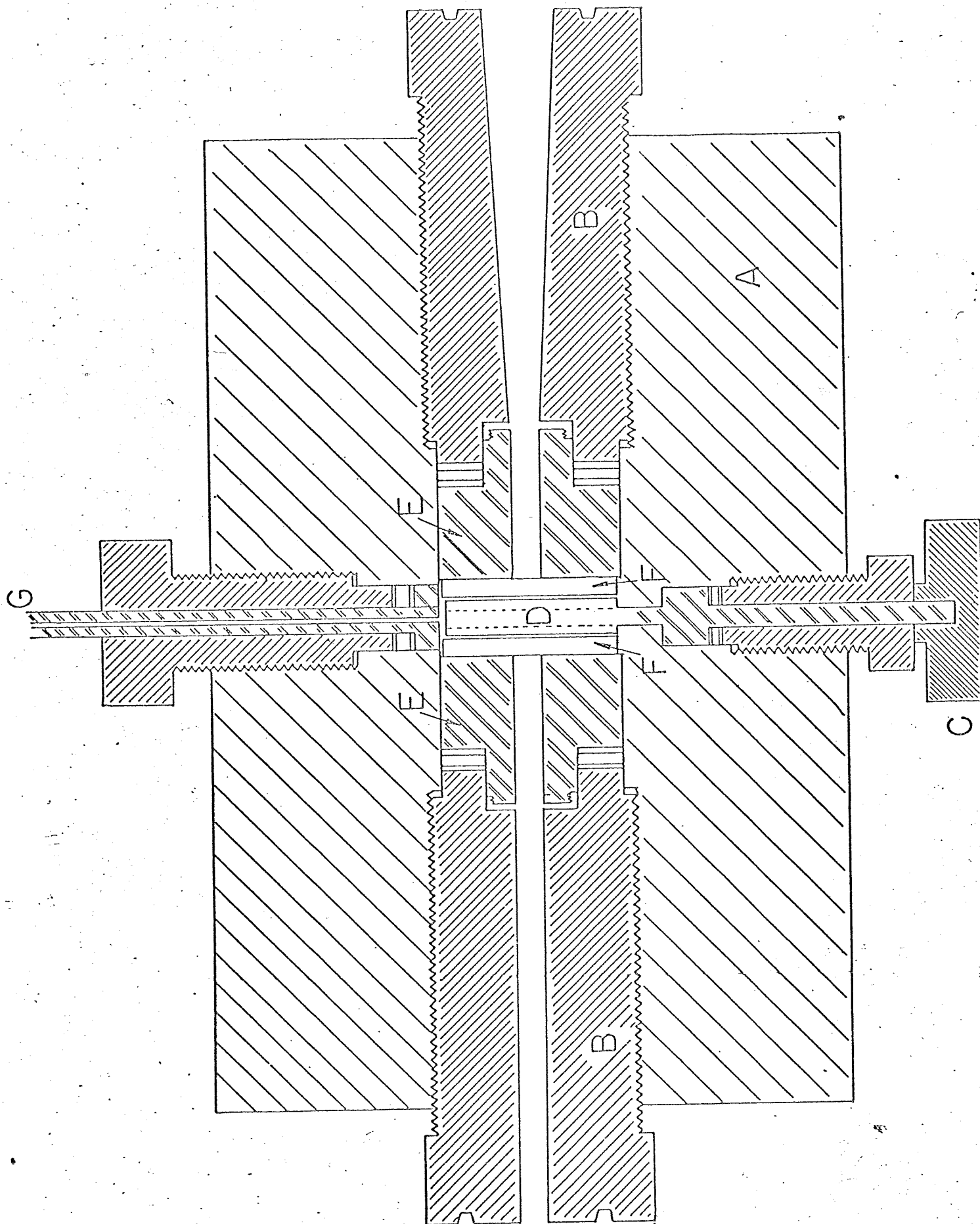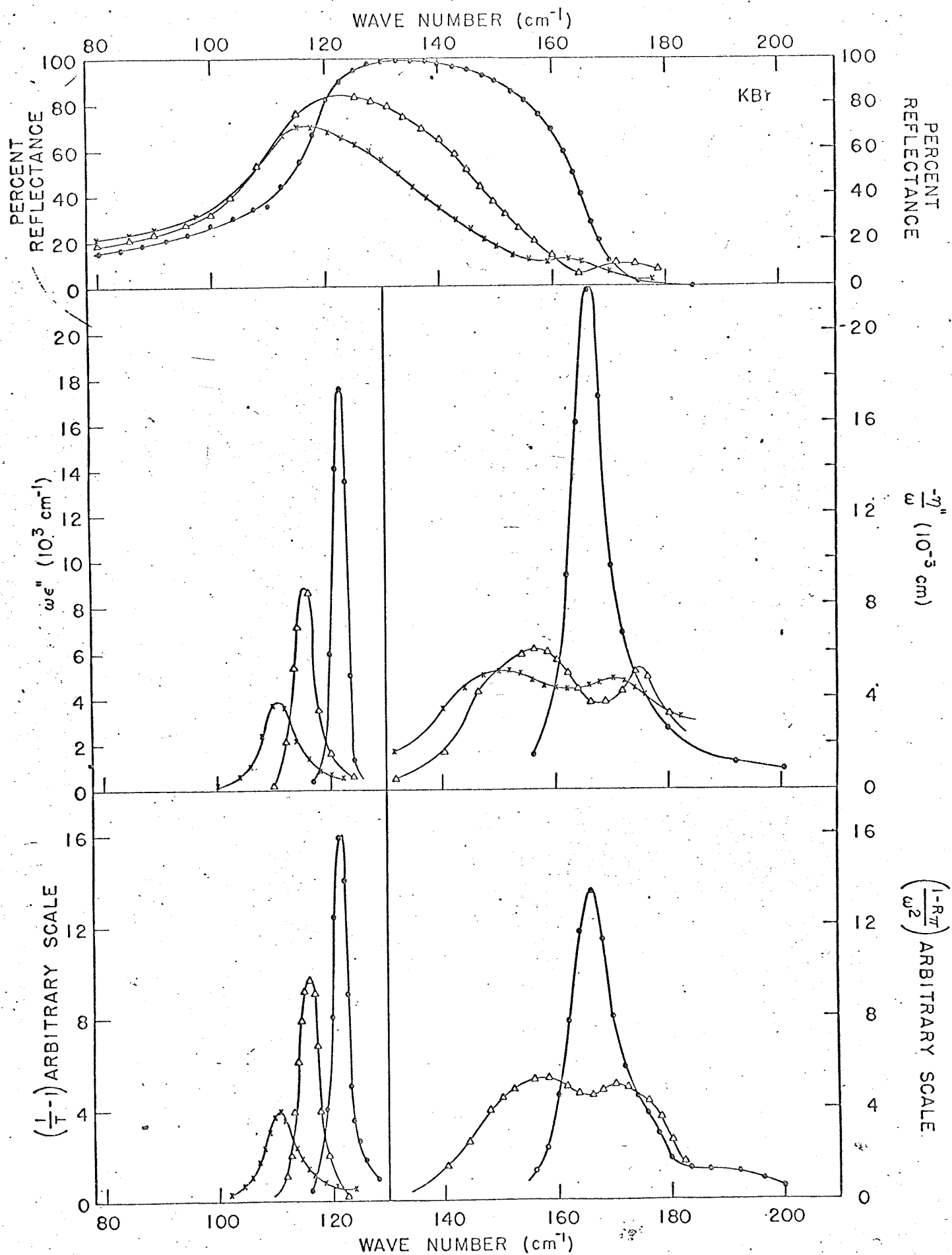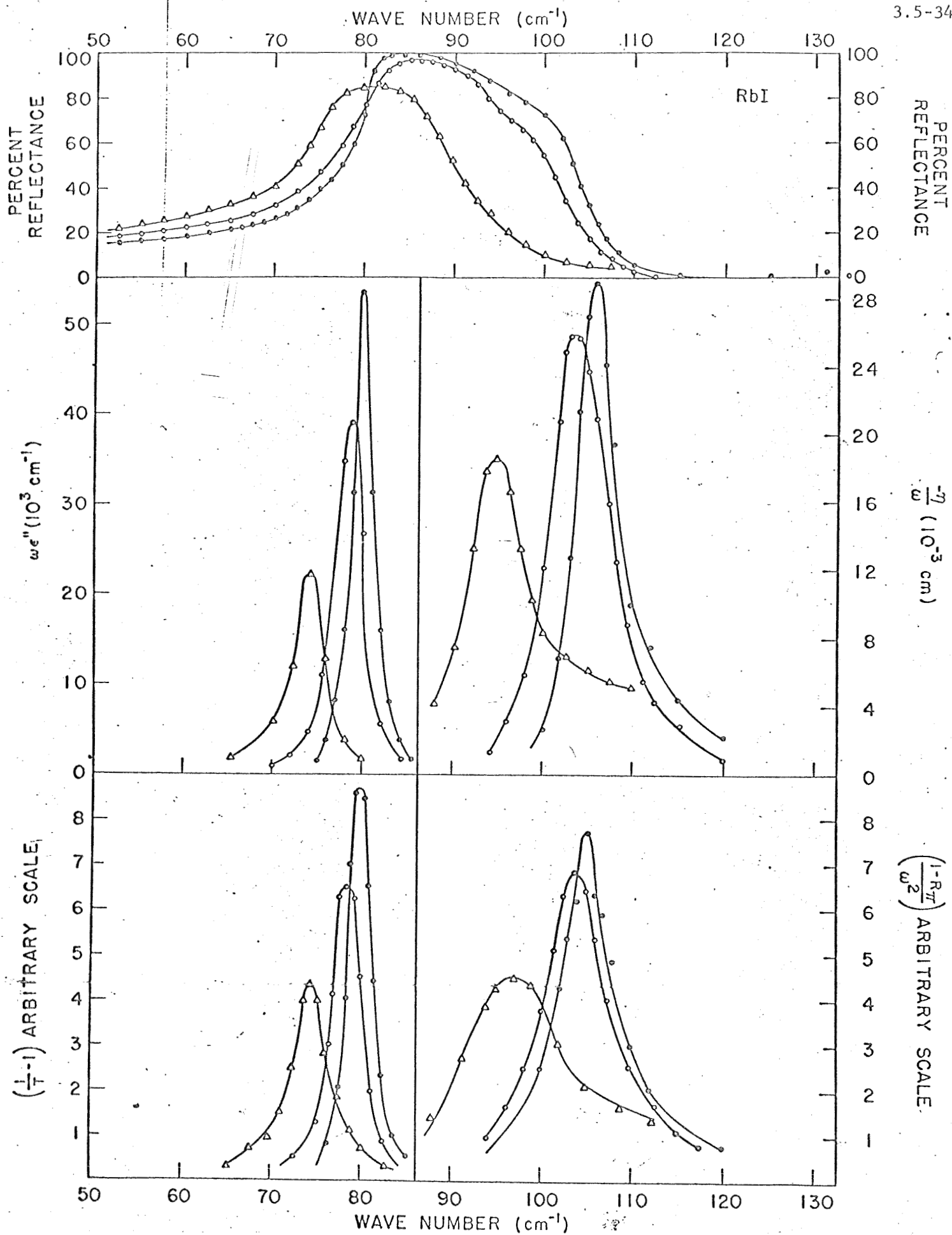
3.6 Silicon Monoxide Bands in Some Low-Temperature Stars

J. H. Fertel

SILICON MONOXIDE BANDS IN SOME LOW-TEMPERATURE STARS

Jeanne H. Fertel

Research Laboratory of Electronics, Massachusetts Institute of Technology
and
Solid State Spectroscopy Laboratory, Physics Department, Northeastern University

ABSTRACT

Several bands which appear in the near infrared spectra of cool stars may be due to SiO.

McCammon, Münch, and Neugebauer (1967) reported that the spectra of many low-temperature stars show two shallow absorption features at approximately 2.11 and 2.16 μ, which had not been identified. These features are strongest in the spectra of late N-type stars.

We suggest that this absorption be assigned to the R-heads of the $\Delta v = 4$ rotation-vibration bands of silicon monoxide. This molecule is predicted by chemical equilibrium calculations to be the most abundant of the heavier molecules in the atmospheres of cool stars (Morris and Wyller 1967). In addition, the SiO absorption bands should be enhanced over those of lighter molecules of similar abundance because of their denser rotational structure. SiO has already been identified in the spectrum of 119 Tau (Knacke et al. 1969) where its fundamental rotation-vibration band is observed at 8.2 μ.

More recent cool-star spectra at higher resolution (approximately 8 cm^{-1}) have been published by Johnson et al. (1968), and show many more features attributable to SiO. The spectra of χ Cyg and Y CVn, shown in Fig. 1, were recorded with a Block Engineering Michelson interferometer placed at the Cassegrainian focus of a 60" aluminum-mirror telescope, and are corrected for atmospheric extinction as described elsewhere (Johnson et al. 1968). Parts of the $\Delta v = 4$, 5, and 6 SiO band sequences are expected to occur in this wave-number region. The positions of the band heads have been calculated and those that

coincide with observed bands are indicated in Fig. 1. Several of the others are predicted to occur in the H_2O region or on top of CO and C_2 bands and are therefore unobservable.

FOOTNOTES AND REFERENCES

*This work was supported in part by the Joint Services Electronics Program (Contract DA28-043-AMC-02536(E)).

Johnson, H. L., Coleman, I., Mitchell, R. I., and Steinmetz, D. L. 1968, Comm. Lunar and Planet. Lab., 113, 83.

Knacke, R. F., Gaustad, J. E., Gillett, F. C., and Stein, W. A. 1969, Ap. J., 155, L189.

McCammon, D., Münch, G., and Neugebauer, G. 1967, Ap. J., 147, 575.

Morris, S., and Wyller, A. A. 1967, Ap. J., 150, 877.

FIGURE CAPTION

Fig. 1. Near infrared spectra of χ Cyg and Y CVn. The SiO rotation-vibration lines are indicated by vertical bars.

X CYG

Y C VN

Δv = 6

Δv = 5

Δv = 4

WAVENUMBERS (cm⁻¹)

7000 6500 6000 5500 5000 4500 4000

INTENSITY (ARBITRARY UNITS)

3.6-5
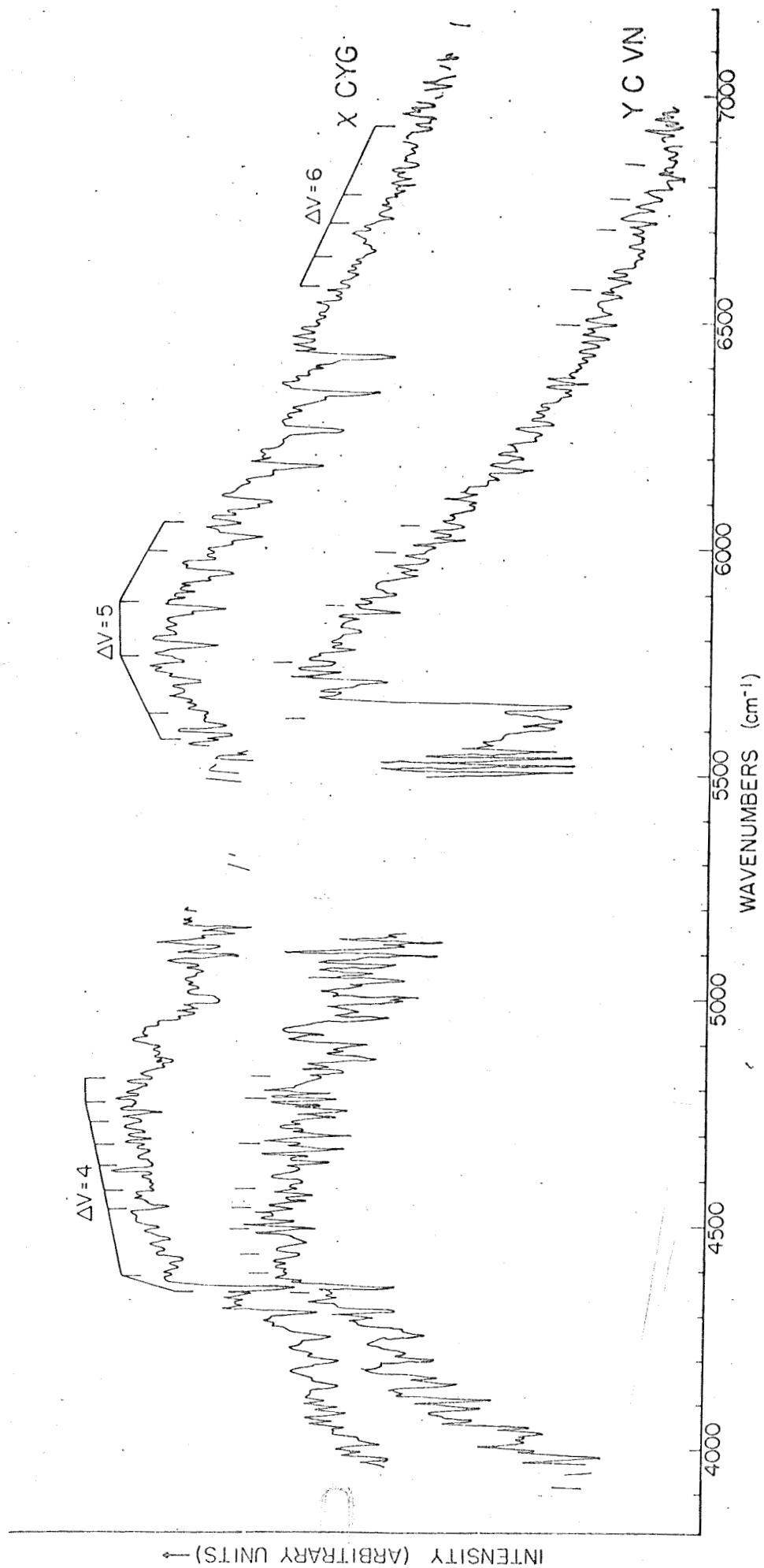
3.7 The Raman Spectra of the Alkali Halides and Some of
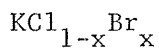
Their Mixed Crystals

J. H. Fertel and C. H. Perry

$KCl_{1-x}Br_x$

The Raman spectra of room temperature $KCl_{1-x}Br_x$ (with $x = 0$, .08, .25, .5, .75, .92 and 1.0) have been observed from 30-400 cm^{-1} frequency shift from the exciting line. Several previous workers have measured and analyzed the KBr spectrum in considerable detail and their experimental results are in qualitative agreement with ours. The KCl spectrum has been reported by Stakhanov and Eliashberg, who also observed the Raman spectra of $KCl_{1-x}Br_x$ with $x = .2$, .4, and .8. Their results do not agree with ours and are considerably less detailed, and no attempt is made to analyze the data.

The Raman spectrum of $KCl_{1-x}Br_x$ for various values of x are shown in Fig. 1. The relative intensity of all the graphs is linear, but they have been slightly shifted for optimum display. The scale for the spectra for which $x \leq .25$ is twice that of the others. The resolution is approximately 7 cm^{-1} in all cases, and the peak positions can be reproduced to within 5 cm^{-1}.

The observed frequencies together with the assignments from this work are tabulated in Table 1. The spectra of the end members have been assigned as described above and our interpretation of the KBr spectrum is roughly the same as that of Burstein et al. The assignments for the intermediate values of x were made by comparison, i.e., it was expected that the peaks in the KCl spectrum would vary smoothly into the KBr peaks as x was increased. This requirement enabled the elimination of many possible combinations. For instance, the KCl band at 292 cm^{-1} could also have been identified with the overtone 2LA(L) (which is predicted to occur at about 302 cm^{-1}). The value of the frequency of this overtone in KBr is 186 cm^{-1}. It can be seen however that there is no peak in the KBr spectrum at this

Table 1 Observed Raman Peaks of $KCl_{1-x}Br_x$

Predicted Frequency (KBr)	Assignment	Observed Frequencies (cm^{-1})							Assignment	Predicted Frequency (KCl)
		x=1	x=.92	x=.75	x=.5	x=.25	x=.08	x=0		
	laser	40.6	39.4	41.5	39	--	37	38		
52	LA-TA(Δ)	58	58.5	69	71	74	83	81	LA-TA(Δ)	77
82	2TA(X)	87	86.5	96,114	--	116	116	121	2TA(X)	116
122	LA+TA(Δ)	126	134	133	138	152	155	182	LA+TA(Δ)	185
144	2LA(X)	142		--	--	212	213	214	2LA(X)	218
161	TO+TA(X)	165.5	--	--	--	--	--	--		
164	TA+LA(L)									
209	LO+LA(Δ)	215	217	224	--	--	--	--		
234	2TO(Δ)	236.5	241		255	276	288	292	2TO(Δ)	290
240	2TO(X)								LO+TO(Δ)	287
239	LO+TO(Δ)								2TO(X)	292

frequency and that, in fact, the KCl band at 292 cm^{-1} goes smoothly into the 236.5 cm^{-1} band of KBr, as x is increased. Thus this particular assignment is ruled out.

It should be noted that the combinations TO-TA(Δ), LO-TA(Δ), and LO-TA(X), and the overtone 2TA(X) all have roughly the same frequency in KBr, although the 2TA(X) frequency is separated from the others is KCl, giving rise to two peaks at x = 0. These two peaks can be seen to slowly converge as x is increased, merging into one when x = .92. It is not clear however whether the 2TA(X) overtone in the x = .75 crystal is represented by the peak at 96 cm^{-1} or that at 114 cm^{-1}.

Similarly the LA+TA(Δ) combination and the 2TA(L) overtone are split only at the x = 1 end of the combination range. The 224 cm^{-1} band of the x = .75 sample is taken to be an unresolved combination of the band due to 2TO(X), LO+TO(Δ), and 2TO(Δ) (which appears at 236.5 cm^{-1} in KBr) and the LO+LA(Δ) band (which appears at 215 cm^{-1} in KBr). This last-named band is not observed in the crystals for which x < .75.

The Raman spectrum of $KCl_{.08}Br_{.92}$ has previously been reported by Murrall, Porto, Damen, and Mascarenhas. They assign the band at 134 cm^{-1} to a first order impurity mode, treating the Cl^{-} ions as non-interacting point defects. The spectra presented here do not support this conclusion however, as the 134 cm^{-1} band is of the same order of magnitude as the other (second order) bands. In any case, 8 mole percent KCl is a rather large amount to be considered as a point impurity.

KC1-KBr Mixed Crystals

1. E. M. Fuller, G. M. Randall and D. J. Montgomery, Bull. Am. Phys. Soc. 9, 644 (1964).

2. A. Mitsuishi in U.S.-Japan Cooperative Seminar on Far Infrared Spectroscopy, Columbus, Ohio, 1965 (unpublished).

3. J. F. Murrell, S. P. S. Porto, T. C. Damen and A. Mascarenhas, Phys. Lett. 26A, 194 (1968).

4. M. M. Krauzman, G. R. Acad. Sc. 265, B1029 (1967).

5. M. Krauzman, in Light Scattering Spectra of Solids, G. B. Wright, ed. Springer-Verleg, New York, 1969, p. 109.

6. A. I. Stokanov and M. B. Blisehberg, Opt. Spectry. (USSR) 10, 174 (1961); Sov. Physics - Solid State 2, 2096 (1961).

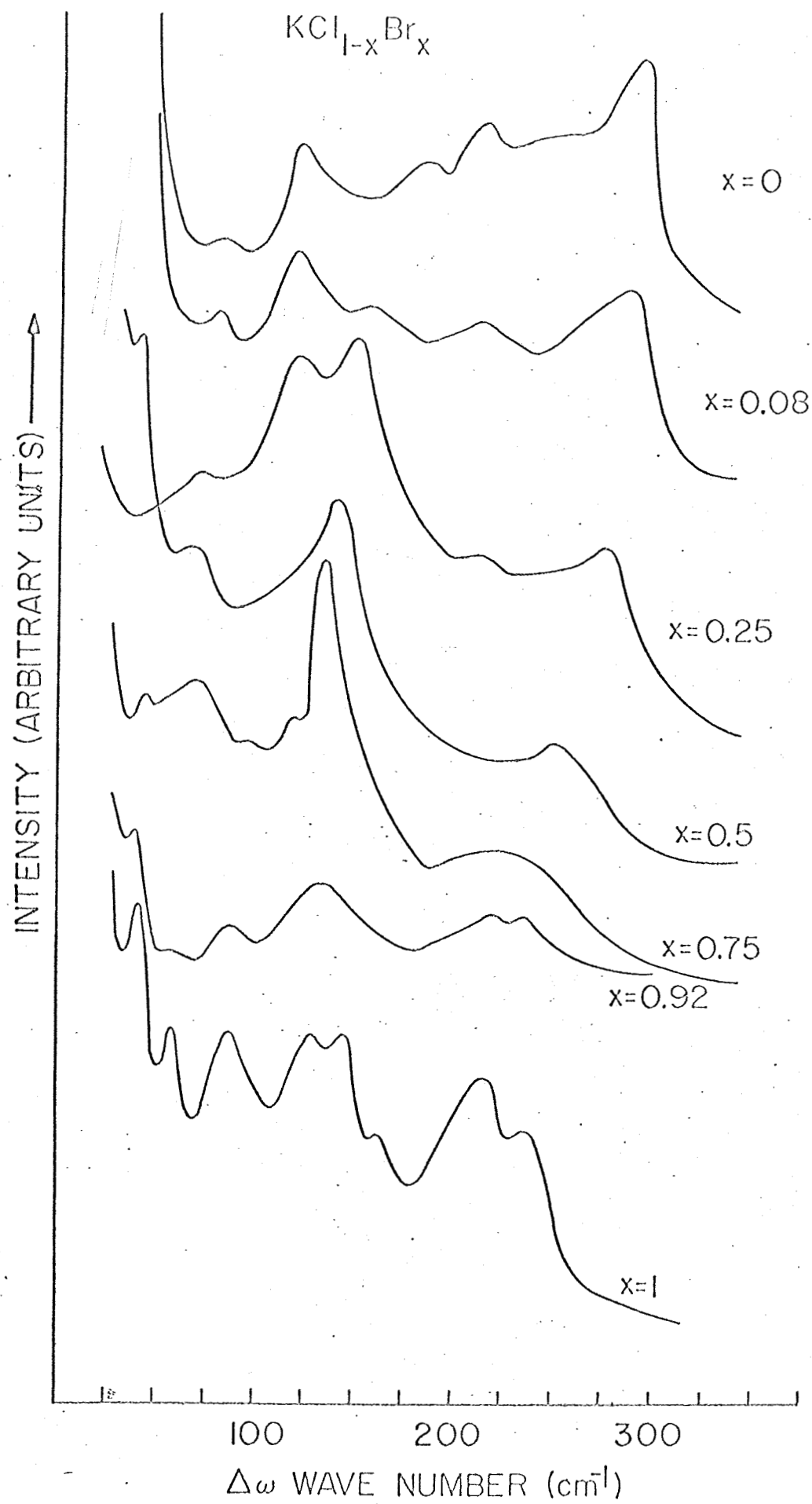7. E. Burstein, P. A. Johnson and Z. London, Phys. Rev. 139, A1239 (1965).

Fig. 1

3.8 Electric Field-Induced Birefringence in Diamond

E. Anastassakis

This work, initiated at the University of Pennsylvania (1968) and completed at the Northeastern University (1969) under the partial support of NASA, deals with quadratic field-induced birefringence in diamond-type crystals. This effect arises from a second order electro-optic effect (true effect), and an electrostriction (false effect). A simple technique was successfully applied for direct measurements of the retardation between an "ordinary" and an "extraordinary" wave emerging from the crystal. It was observed that the particular diamond sample that we used in this experiment, exhibited a residual birefringence, due to an estimated average residual strain of $\sim 10^{-5}$. The experimental measurements revealed the existence of a linear effect, related to the history of the sample through its imperfections, e.g., residual strains, impurity, etc. The linear and nonlinear effects were separated and a numerical value for one of the nonlinear electro-optical coefficients was found to be equal to $\left| z^{E}_{1212} \right| \simeq 8 \times 10^{-18} \left(\frac{cm}{V} \right)^{2}$. It turned out that the "false" effect did not exceed 1% of the "true" effect, and that the relative change of the dielectric constant of an ideal non-birefringent diamond crystal with a static electric field in second order, is of the order of 10^{-6} for an applied field of 2×10^{5} V/cm.

4. Summary

The results presented in this report indicate that the majority of objectives were accomplished and the results have been interpreted in a satisfactory manner. There remains, however, a considerable number of un-answered questions, both experimental and theoretical and it is hoped that this work will continue with the appropriate financial support. The rescinding of the continued support for this work at the current level due to the closing of the Electronics Research Center is unfortunate. It would be hoped that while this grant is apparently going into a step-funding phase some other interested parties within the NASA organization would appreciate the extent of the work and effort that has gone into the program so far and the large amount of data and results that have been produced. Consequently, it would be highly desirable for this program to be reinstated so that the personnel involved could continue and that the work would proceed with the same momentum.

This group consisting of Professors Perry, Lowndes and Anastassakis have many ideas on the spectroscopic investigation of materials exhibiting properties such as ferroelectricity, piezoelectricity, antiferromagnetism, nonlinear effects, crystalline Stark effects, Zeeman splitting and electro- and magneto-optic effects and morphic effects. The study of these effects under the influence of temperature, pressure, electric and magnetic fields, etc., are of basic scientific interest as well as disclosing useful data for predicting general engineering applications. Consequently, it is to this end that we believe that these measurements should be continued in the future.

This work is also extremely germane to the continuation of our graduate research program in this area.

APPENDIX A

A1. Academic and Research Staff

        The following research workers contributed to the research reported

in this annual report:

        Professor C. H. Perry* (principal investigator)

        Professor R. P. Lowndes (associate investigator)

        Professor E. Anastassakis (associate investigator)

        Dr. Jeanne H. Fertel (visiting research associate)

        Dr. J. F. Parrish (visiting research associate)

        Mr. N. E. Tornberg (visiting research associate)

        Mr. D. K. Agrawal* (graduate research assistant)

        Mr. H. C. Hwang* (graduate research assistant)

        Mr. H. C. Cronin (technical assistant)

        Mr. J. Sanroma (technical assistant)

        *Supported directly by this grant. Others supported in part.

Degrees Granted

        Jeanne H. Fertel - Ph.D., Physics (M.I.T.), August 1969.

        J. F. Parrish - Ph.D., Physics (M.I.T.), October 1969.

A2. Related Contracts

        This work was also supported in part by the Joint Services

Electronics Program (U.S. Army, U.S. Navy and U.S. Air Force) under contract

DA 28-043-AMC.-02536 (E) at M.I.T., and by the U.S. Air Force (ESD Contract

AF 19(628)-69-C-0081) at Northeastern University.

        A Northeastern grant (3390-9910) for Basic Research is also

gratefully acknowledged.

A3. <u>Acknowledgments of Facilities</u>

The continuous facilities of the Research Laboratory of Electronics, M.I.T., and the Spectroscopy Laboratory at M.I.T., during the early part of the transition to Northeastern University were much appreciated.

The availability and facilities of the Francis Bitter National Laboratory are also gratefully acknowledged.

Finally, we wish to show our appreciation for the loan of equipment from the NASA Electronics Research Center, Cambridge, Mass., without which a large amount of this work would not have been possible. In particular, we would like to thank Dr. F. Haak (of ERC) for his continued help and interest in this work and for supplying some of the materials under investigation.

APPENDIX B

Publications and Activities Sponsored in Part by This Grant

Optical Phonons and Phase Transitions in the Ammonium Halides. - C. H. Perry
and R. P. Lowndes, J. Chem. Phys. 51, 3648 (1969).

The Raman Spectrum of Ferroelectric SbSI. - C. H. Perry and D. K. Agrawal,
Solid State Comm. 8, 225 (1970).

A Variable Temperature (8-400°K) Gas Transfer Cell for Solid State
Spectroscopy. - N. E. Tornberg and C. H. Perry, Applied Optics 9, 777
(1970).

Far Infrared Stark and Zeeman Splittings of Er^{3+} in the Lanthanide Fluorides. -
J. F. Parrish, C. H. Perry and R. P. Lowndes, Phys. Letters 31A, 262
(1970).

Raman Spectra of Alkali Halides and Some of Their Mixed Crystals. -
Jeanne H. Fertel and C. H. Perry, Proc. Symp. on Molecular Structure and
Spectroscopy, Ohio State University, Columbus, Ohio, Sept. 2-6, 1969,
Paper T-3. Abstracts p. 87.

Measuring Uniaxial Spectral Dielectric Response: Application to Calcite
$CaCO_3$ and Tysonite LaF_3. - J. F. Parrish and C. H. Perry, Proc. Symp.
on Molecular Structure and Spectroscopy, Ohio State University,
Columbus, Ohio, Sept. 2-6, 1969, Paper T-4. Abstracts p. 88.

Optical Phonons and Phase Transitions in Thallous Iodide. - R. P. Lowndes
and C. H. Perry, Proc. Symp. on Molecular Structure and Spectroscopy,
Ohio State University, Columbus, Ohio, Sept. 2-6, 1969, Paper T-5.
Abstracts p. 88.

The Influence of Lattice Anharmonicity on the Longitudinal Optic Modes of
Cubic Ionic Solids. - R. P. Lowndes, Phys. Rev. (in press).

Silicon Monoxide Bands in Some Low-Temperature Stars. - Jeanne H. Fertel,

    Astrophysical Journal $\underline{159}$,   L7   (1970).

Temperature Independent Optical Phonons in Lead Titanate. - N. E. Tornberg

    and C. H. Perry, J. Chem. Phys. (in press).

Resonance Raman Scattering from Electron Gas Excitations at the $E_o + \Delta_o$

    Energy Gap of GaAs. - A. Pinczuk, E. Burstein, L. Brillson and

    E. Anastassakis, Bull. Am. Phys. Soc. $\underline{15}$, 327 (1970).

The Effect of Time Reversal Symmetry on $q \simeq$ Optical Phonons. - E. Anastassakis

    and E. Burstein (to be published).

APPENDIX C

Suggested Distribution List

Professor P. L. Richards
Physics Department
University of California
Berkeley, California 94720

Professor A. J. Sievers
Laboratory of Atomic & Solid State Physics
Cornell University
Ithaca, New York 14850

Dr. Ely Bell
Laboratory of Molecular Spectroscopy & Infrared Studies
Department of Physics
Ohio State University
Columbus, Ohio 43210

Dr. Marvin Haas
Naval Research Laboratories
Washington, D.C. 20390

Dr. A. S. Barker, Jr.
Bell Telephone Laboratories
Murry Hill, New Jersey 07974

Dr. Eli Burstein
Department of Physics
University of Pennsylvania
Philadelphia, Pennsylvania 19104

Dr. H. Caspers
Naval Weapons Center Corono Laboratories
Corona, California 91720

Dr. R. Buchanan
Research Laboratory
Lockheed Missiles & Space Company
Palo Alto, California 94304

Dr. S. Zwerdling
Macdonnel Douglas Research Laboratory
Huntington Beach, California

Dr. J. M. Dowling
Space Physics Laboratories
Aero-Space Corporation
Los Angeles, California 90045

Dr. G. Rupprecht
Bendix Research Corporation
Englewood, Colorado 80110

Dr. W. Fateley
Mellon Institute
Pittsburgh, Pennsylvania 15213

Professor R. Wheeler
Department of Physics
Yale University
New Haven, Connecticut 06520

Dr. R. Hill
General Motors Research Laboratories
Warren, Michigan 48090

Professor J. R. Durig
Department of Chemistry
University of South Carolina
Columbia, South Carolina 29208

Dr. W. Lafferty
National Bureau of Standards
Gaithersburg, Maryland 20760

Professor J. R. Hardy
Department of Physics
University of Nebraska
Lincoln, Nebraska 68508

Dr. George Wilkinson
Physics Department
Kings College
University of London
London, W.C.2, England

Professor Derek H. Martin
Physics Department
Queen Mary College
Mile End Road
London, E.1, England

Professor L. Genzel
Physikalisches Institut
University of Freiburg
Freiburg, Germany

Dr. A. Hadin
University of Nancy
Institut de Physique
Nancy, France

Professor H. Yoshimaga
Department of Applied Physics
Osaka University
Osaka, Japan

Dr. A. Johnson
Royal Radar Research Establishment
Melvern
Worcestershire, England

Dr. J. Chantry
National Physical Laboratory
Teddington
Middlesex, England

Dr. T. Nakamura
Institute for Solid State Physics
University of Tokyo
Acabu Shinrydo-Cho
Tokyo, Japan

Professor W. Cochran
Department of Natural Philosophy
University of Edinburgh
Edinburgh, U.K.